Spontaneous Ca^{2+} signals in adult-born juxtaglomerular neurons during their integration into the glomerular layer of the mouse olfactory bulb

Thesis submitted as requirement to fulfil the degree “Doctor of Philosophy (Ph.D.)”

at the

Faculty of Medicine

Eberhard Karls University

Tübingen

by

Anatoliy Maslyukov

from

Odessa, Ukraine

2018

Dean:	Professor Dr. I.B. Autenrieth
1. Reviewer	Professor Dr. O. Garaschuk
2. Reviewer	Professor Dr. S. Liebau

I dedicate this thesis to my grandmother Nadiya Mazur, who was encouraging me to study medicine and support my desire to become a scientist.

Table of contents

List of abbreviations

BrdU	5-bromo-3’-deoxyuridine
Dcx	doublecortin
DG	dentate gyrus
DPI	day post injection
eGFP	enhanced green fluorescent protein
ETC	external tufted cells
FRET	Förster resonance energy transfer
GAD	glutamic acid decarboxylase
GL	glomerular layer
IQR	interquartile range
JGNs	juxtaglomerular neurons
LSM	laser scanning microscopy
OB	olfactory bulb
PBS	phosphate-buffered saline
PGCs	periglomerular cells
PMT	photomultiplier tubes
PSA-NCAM	polysialylated neuronal cell adhesion molecule
RMS	rostral migratory stream
SA	short axon cells
SVZ	subventricular zone
TH	tyrosine hydroxylase
TTX	tetrodotoxin

Introduction

"…once development was ended, the founts of growth and regeneration of the axons and dendrites dried up irrevocably. In the adult centres the nerve paths are something fixed and immutable: everything may die, nothing may be regenerated…"

Santiago Ramón y Cajal

During the end of the 20th century neuroscience has witnessed the revision of long lived dogma. Since the origins of the neuronal doctrine for more than 100 years it was believed that neurogenesis occurs only during development, and new neurons are not added to the mammalian brain.

This belief was first challenged after introduction of [^{3}H]-thymidine autoradiography. Using this method Josef Altman acquired data showing new neurons in the dentate gyrus (DG) of the hippocampus and olfactory bulb (OB) of the postnatal and adult rats [Altman et al. 1965; Altman, 1969]. Michael Kalpan using electron microscopy showed that cells labelled with [^{3}H]-thymidine in the olfactory bulb and dentate gyrus of adult rats have ultrastructural characteristics of neurons [Kaplan et al. 1977; Kaplan et al. 1984]. Next convincing evidence came from the studies in which synthetic analogue of thymidine BrdU (5-bromo-3'-deoxyuridine) was used as marker of dividing cells and their progeny [Kuhn et al. 1996; Kempermann et al. 1997]. Using combination of BrdU labelling with labelling against cell-type specific neurochemical markers, such as polysialylated neuronal cell adhesion molecule (PSA-NCAM) and doublecortin (Dcx) researchers proved that BrdU-positive cells in the adult rodent brain indeed were immature neurons [Bonfanti et al. 1994; Seki 2002; Brown et al. 2003]. BrdU labelling was used to show adult neurogenesis in different mammalian species including humans [Eriksson et al. 1998].

Under the normal conditions adult neurogenesis is limited to the two neurogenic areas of the rodent brain – dentate gyrus of the hippocampus and neurogenic system of the olfactory bulb that includes olfactory bulb (OB) itself, subventricular zone (SVZ) and rostral migratory stream (RMS).

Olfactory bulb and its neurogenic system

Olfactory system detects airborne molecules, called odorants, providing an organism with chemical information about environment and other species. Olfactory information triggers essential behavioural responses, such as: feeding behaviour, predator avoidance, social interactions, reproduction.

Odorants interact with olfactory sensory neurons (OSNs) that are located in the olfactory epithelium of the nasal cavity. Axons of the OSNs form olfactory nerve that enters the olfactory bulb where they make synapses with apical dendrites of principal projection neurons of the OB called mitral cells (MCs). Contacts between the axons of OSNs and apical dendrites of MCs found in the glomerular layer of the OB and organized in spherical accumulations of neuropil called glomeruli. OSNs expressing same type of odorant receptor send their axons to one or two odorant-receptor type specific glomeruli in each OB.

Glomeruli, that are located on the surface of the OB represents first processing centre of this system. In each glomerulus huge number of axons of the OSNs expressing same type of the olfactory receptor converge on the apical dendrites of the few MCs. Usually OSNs having same type of the olfactory receptor targets two glomeruli in each olfactory bulb, one on the medial side of the OB and one on the lateral [Wachowiak et al. 2006]. This input is modulated by the local circuit of juxtaglomerular neurons (JGNs). Cell bodies of JGNs surround each globular accumulation of the neuropil that contains synaptic connections between axons of OSNs, apical dendrites of MCs and dendrites of JGNs. The population of JGNs is comprised of 3 morphological classes: external tufted cells, short axon cells and periglomerular cells (PGCs).

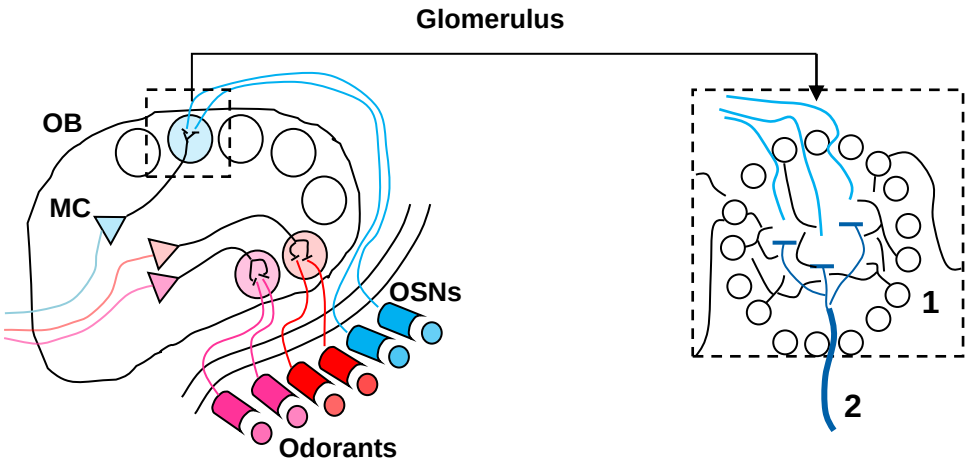

Figure 1. Schematic representation of the signal-processing circuitry of the olfactory bulb. OB – olfactory bulb; MC – mitral cell; OSNs – olfactory sensory neurons; 1 – juxtaglomerular neurons; 2 – dendrite of the mitral cell.

PGCs are the most numerous subpopulation of JGNs [Lepousez et al. 2013]. These cells are GABAergic interneurons with some of them being GABAergic/dopaminergic. They send their dendrites into one or two neighbouring glomeruli. PGCs form GABAergic synapses with the dendrites of MCs inhibiting their response to the inputs from OSNs. Depending on synaptic relationship of PGCs with axons of OSNs and apical dendrites of the MCs inside of a given glomerulus, PGCs provide feed-back or feed-forward inhibition to the intraglomerular processing circuit [Wachowiak et al. 2006].

Short axon cells, being predominantly GABAergic/dopaminergic [Kiyokage et al., 2010], are responsible for long distance connections inside of the glomerular layer. These cells play important role in interglomerular lateral inhibition, enhancing contrast between weakly and strongly activated glomeruli [Wachowiak and Shipley 2006].

Output from mitral cells is modulated by the circuit of GABAergic interneurons called granule cells. Granule cells make reciprocal dendro-dendritic contacts with lateral dendrites of the mitral cells. They are responsible

for later inhibition between differently activated mitral cells, playing important role in discrimination between similar odorants.

Important part of the signal processing system of the olfactory bulb is comprised of centrifugal inputs coming from different areas of the brain [Shepherd et al. 2004; Kiselycznyk et al. 2006; Mouret et al. 2009]. Most of these inputs target granule cells [Macrides et al. 1981] but JGNs also receive centrifugal inputs [Petzold et al. 2009; Lazarini and Lledo 2011] that provide contextual information to initial steps of olfactory information processing.

Mitral cells send projections into the pyriform cortex in the temporal lobe of the brain and pyriform cortex, in turn, relay olfactory information to the associative area of the neocortex via the thalamus.

Thus, odorant binding to the specific receptors on the OSNs initiates flow of the information through the olfactory system leading to an appropriate behavioural response.

Adult neurogenesis in the olfactory bulb

Neuronal progenitors destined for OB are born in the subventricular zone and in the rostral migratory stream [Guillemot and Parras, 2005]. SVZ is a region that placed along the walls of the lateral ventricles of the brain and RMS is a pathway connecting SVZ with the olfactory bulb. After their birth, neuronal progenitors sliding along each other towards the olfactory bulb forming in such way chains of migrating neuroblasts. These chains are encapsulated by glial cells preventing them from dispersion into surrounding tissue. Several thousands of adult-born cells enter into the rodent OB every day [Lledo et al. 2006]. Upon arrival into the olfactory bulb neuroblasts detach from the chains and start radial migration into their target layers inside of the OB. Most of these cells will settle in the deep layer of the OB to become granule cells but some of them, approximately 5% will migrate further into the superficial layer of the OB to become JGNs [Lledo et al. 2006]. Among JGNs adult neurogenesis contributes mostly to the sub-population of inhibitory periglomerular neurons

[Lepousez et al. 2013] with very limited fraction giving rise to glutamatergic short axon cells [Brill et al. 2009].

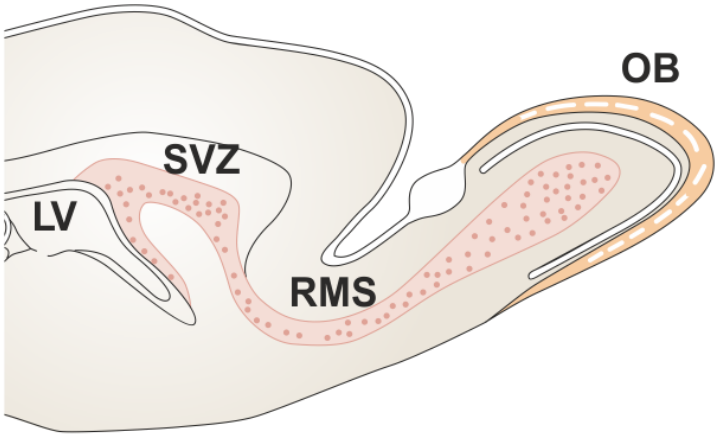

Figure 2. Schematic representation of the neurogenic system of the olfactory bulb. (Modified from [Lledo et al. 2006]). LV – lateral ventricles of the brain; SVZ – subventricular zone; RMS – rostral migratory stream; OB – olfactory bulb.

In the rodent olfactory bulb there are approximately 1.2 millions of JGNs [Parrish-Aungst et al. 2007]. Fraction of adult-born JGNs increases with age reaching approximately 30% of cells over the period of 9 months whereas fraction of adult-born granule cells is maintained throughout the life of an animal at relatively constant level of approximately 12% of cells [Ninkovic et al. 2007].

Introduction of virus-based linage tracing method provided a possibility to study development of adult-born granule cells and JGNs during their integration into corresponding mature neuronal circuits. Injection of viral vectors encoding fluorescent proteins into the subventricular zone or into the RMS results in labelling of adult born neurons arriving into the OB that can be visualized in fixed slices and in living brain tissue.

Adult-born granule cells require approximately 4 weeks to develop morphology similar to surrounding preexisting neurons [Petreanu et al. 2002]. Studies in acute brain slices that took an advantage of combination virus-based linage tracing with electrophysiological techniques showed that after this maturational period adult-born granule cells acquire intrinsic membrane properties similar to their preexisting counterparts [Carleton et al. 2003].

Recordings of spontaneous synaptic events in developing adult-born granule cells showed that they start to form synapses during the second week after viral injection into the SVZ with GABA-ergic inputs appearing before glutamatergic ones. Studies of the synaptic connectivity of adult-born granule cells revealed that development of input synapses preceded the development of their output synapses [Whitman et al. 2007b; Kelsch et al. 2008; Panzanelli et al. 2009].

Ability to fire action potential is was evident only in those adult-born granule cells that already develop mature morphology and intrinsic membrane properties [Carleton et al. 2003]. Thus, after their arrival into granule cell layer, adult-born granule cells have to go through the sequence of maturational events that takes approximately 4 weeks-long before start to be able to influence ongoing signal processing that takes place in surrounding mature neuronal circuit.

Morphological development of adult-born JGNs was studied in vivo [Mizrahi 2007] using combination of virus-based linage tracing method and two-photon laser scanning microscopy (LSM). It was shown that 10 days after viral injection into the subventricular zone adult-born JGNs have immature morphology. Most of the adult-born JGNs at 10 days post-injection (DPI) had smooth dendrites and few had spines. At 45 DPI adult-born JGNs showed mature morphology similar to surrounding preexisting neurons. Electrophysiological studies in acute brain slices showed that at the age of 7-14 DPI after viral injections into the RMS adult-born JGNs had immature intrinsic membrane properties and reach mature values at DPI 45 [Grubb et al. 2008]. Action potential firing recorded in acute brain slices was possible for adult-born JGNs already at DPI 7. At the age of DPI 7-14 46% of studied adult-born JGNs were able showed responses to stimulation of the olfactory nerve. Recordings of spontaneous synaptic events revealed similar sequence of input formation with what was seen during the maturation of adult-born granule cells where GABAergic inputs appeared before glutamatergic ones. Synaptogenesis of adult-born JGNs during their integration into the circuit was studied using viral vectors encoding fluorescent protein fused to postsynaptic density scaffold protein PSD-95 [Livneh et al. 2009]. This study revealed that immature DPI 12-

14 adult-born JGNs are characterized by highly dynamic rearrangement of glutamatergic synaptic input whereas at DPI 40-60 these cells showed more stable synaptic contacts.

In vivo evidence showing that adult-born JGNs are indeed involved in the processing of olfactory information were acquired in experiments combining such techniques as: virus-based linage tracing, two-photon-targeted electrophysiological recordings and two-photon imaging of intracellular calcium concentration [Livneh et al. 2014; Kovalchuk et al. 2015]. Action potential firing and increase in intracellular calcium concentration in adult-born JGNs were recorded in response to odorant presentation. Adult-born JGNs neurons were able to respond to physiologically relevant stimuli in vivo approximately two days after their arrival into the glomerular layer of the olfactory bulb. Response profiles of immature adult-born JGNs to different concentration of odorants were similar to the ones that were measured from surrounding pre-existing neurons with exception only for the lowest odorant concentration tested [Kovalchuk et al. 2015].

Thus, in contrast to what was reported for the development of adult-born granule cells, adult-born JGNs start to be involved in signal processing at the glomerular layer of the olfactory bulb soon after their arrival, and being still immature in terms of their morphology, intrinsic membrane properties, expression of neurochemical markers and migrating behaviour.

Adult neurogenesis is a part of neuronal plasticity allowing brain to adapt its performance to environmental challenges and changings in the internal states. Adult neurogenesis in the olfactory bulb is upregulated in female mice after mating, during gestation and lactation [Shingo et al. 2003; Kopel et al. 2012]. It was suggested that adult-born neurons are involved in innate olfactory-driven behaviour such as predator avoidance [Sakamoto et al. 2011]. Adult-born granule cells and JGNs receive centrifugal inputs providing contextual information to the signal processing that takes place in the olfactory bulb [Whitman et al. 2007; Kelsch et al. 2008; Lazarini and Lledo 2011]. Thus, these cells integrate information of different modalities that is important part of a learning process and memory formation. Indeed, it was shown that different

paradigms of olfactory learning lead to upregulation of adult neurogenesis in the olfactory bulb, while, simple exposure to the odorants did not alter neurogenesis [Alonso et al. 2006; Mouret et al. 2008; Moreno et al. 2009]. Experiments aimed to selectively activate adult-born neurons in the olfactory bulb by the means of optogenetics in-vivo showed that this manipulation lead to increase in olfactory learning and memory [Alonso et al. 2012].

It was mentioned above that thousands of neuroblasts arrive into the adult rodent olfactory bulb each day. But only approximately half of them will survive over the integration period [Petreanu et al. 2002]. Those that survive will stay in the bulb for more than a year [Winner et al. 2002]. Enriched sensory input and olfactory learning lead to increased survival and enhanced synaptogenesis of adult-born neurons in the olfactory bulb [Rochefort et al. 2002; Alonso et al. 2006; Mouret et al. 2008; Livneh et al. 2009; Moreno et al. 2009] whereas odorant deprivation results in impaired synaptic development [Kelsch et al. 2009] and decreased survival of adult-born neurons [Mandairon et al. 2003; Yamaguchi et al. 2005; Mandairon et al. 2006].

There is a special time-window in the development of adult-born neurons when these cells are sensitive to the level of sensory input in terms of their survival. Olfactory learning did not altered number of 11 days old adult-born granule cells while increasing survival rate of 18-, 23-, and 30-days old neurons [Mouret et al. 2008]. Comparison of adult-neurogenesis in anosmic mice with normal animals showed that sensory input is of critical importance for survival of adult-born granule cells during the period between 15 and 45 days after their labelling. But at the age of 15 days, time when these cells already arrive into granule cell layer and start to receive synaptic inputs, number and morphology of adult-born granule cells were similar in anosmic and normal mice [Petreanu et al. 2002; Grubb et al. 2008]. Sensory deprivation by cauterization of one nostril of the mouse lead to decrease in the number of adult-born granule cells at the age of 28 days whereas at the age of 14 days number of adult-born granule cells was similar for deprived and not deprived olfactory bulbs [Yamaguchi et al. 2005].

Upon arrival into the glomerular layer of the olfactory bulb immature adult-born cell start lateral migration inside of this layer to achieve final positioning [Liang et al. 2016]. This process can be considered as part of the integration process because a lot of these cells start to be involved in signal processing being still migrating inside of the glomerular layer [Kovalchuk et al. 2015]. In vivo monitoring of the movement of immature adult-born JGNs by the means of two-photon laser scanning microscopy revealed no effect of sensory deprivation on their migratory behaviour [Liang et al. 2016]. Thus, initial steps of integration of adult-born neurons can be guided not only by external sensory inputs but, also by some intrinsic signals of these migrating immature cells.

In developing nervous system spontaneous intracellular Ca^{2+} transients are involved in regulation of migration of neuronal precursors and their subsequent maturation [Rosenberg and Spitzer, 2011]. In contrast to embryonic development, adult-born neurons have to integrate themselves into mature environment. Spontaneous calcium signals were shown to be present in adult-born neuroblasts migrating in the rostral extension of the RMS, in acute brain slices [Darcy et al. 2009].

However, it was not yet studied whether spontaneous calcium signals are present in immature adult-born JGNs during their integration into appropriate mature circuit in vivo.

To achieve this goal, we chose glomerular layer of the mouse olfactory bulb as model system for in vivo experiments. Olfactory bulb is located just beneath the skull and craniotomy over the OB followed by a window implantation with subsequent two-photon calcium imaging provides unique opportunity for visualization of spontaneous Ca^{2+} transients in adult-born JGNs with single cell resolution in vivo, in awake state of the animal.

Aims of this research project:

- To characterize in-vivo the properties of spontaneous Ca^{2+} transients in immature adult-born JGNs during the time-period of their integration into the adult glomerular circuitry
- To study whether spontaneous Ca^{2+} transients in immature adult-born JGNs are sensitive to voltage-gated Na^{+} channels blocker tetrodotoxin (TTX)
- To reveal whether immature adult-born JGNs showing spontaneous Ca^{2+} transients in awake state are able to produce odorant-evoked responses
- To study developmental aspects of spontaneous calcium signalling and neurochemical marker expression in immature adult-born JGNs

Materials and methods

All experimental procedures involving the handling and use of mice were performed in accordance with Institutional Animal Welfare Guidelines and were approved by the state government of Baden-Württemberg, Germany.

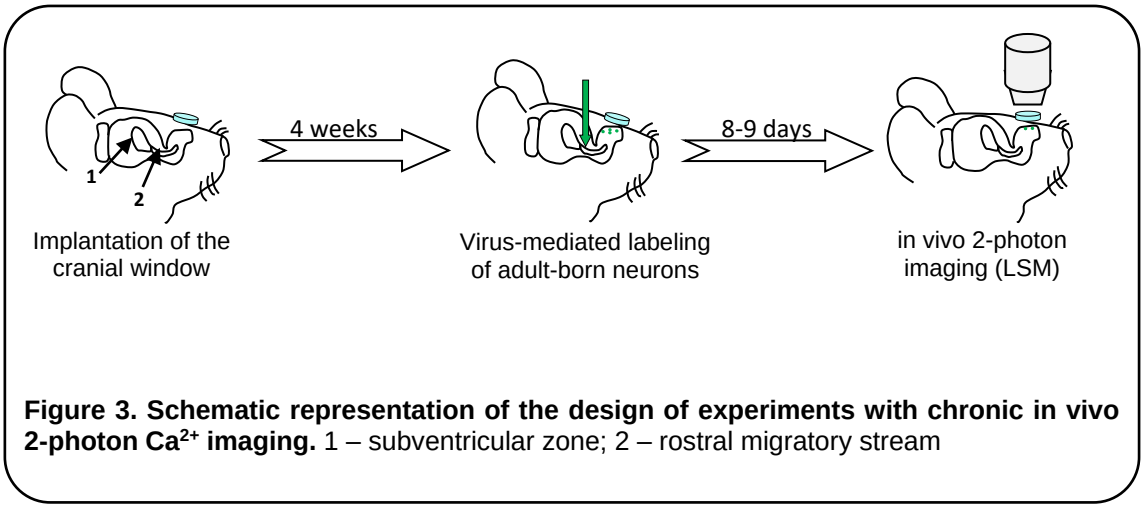

Figure 3. Schematic representation of the design of experiments with chronic in vivo 2-photon Ca^{2+} imaging. 1 – subventricular zone; 2 – rostral migratory stream

Implantation of the cranial window

Male and female 3-6 months old C57/BL6 mice were used for cranial window implantation. Mice were anesthetized with intraperitoneal (i.p.) injections of ketamine/xylazine (80/4 µg/g body weight (BW)). Ketamine, (Fagron, Barsbuettel, Germany), and xylazine (Sigma-Aldrich, St. Louis, MO, USA). Bepanthen (Bayer, Germany) was applied on the eyes of the mouse to prevent dehydration. Before the beginning of the surgery dexamethasone was administered via intraperitoneal (i.p.) injection at the concentration of 2 µg/g BW (Sigma-Aldrich, St. Louis, MO, USA). During the surgery depth of the anesthesia was monitored by toe pinch and additional ketamine/xylazine (40/2 µg/g of BW) was injected when necessary. Temperature of the mouse was monitored with rectal temperature probe connected to the digital thermometer.

During the surgery, and until full recovery the mouse was kept on a heating plate with temperature 37-38 °C.

Prior to the removal of the skin over the OB lidocaine 2% (AstraZeneca, Wedel, Germany) was applied subcutaneously. After removal of the skin above the olfactory bulbs, the skull was cleaned and dried. A circular groove in the skull covering both olfactory bulbs was done using a microdrill and thinned skull over each olfactory bulb was removed with fine tweezers, leaving the dura intact. The opening was rinsed with the standard extracellular solution of following composition 125 mM NaCl, 4.5 mM KCl, 26 mM $NaHCO_3$, 1.25 mM NaH_2PO_4, 2 mM $CaCl_2$, 1 mM $MgCl_2$ and 20 mM glucose, pH 7.4, bubbled continuously with 95% O2 and 5% CO2.

Both olfactory bulbs were covered with a single circular coverslip 3 mm in diameter (Warner Instruments, Hamden, CT, USA). Cyanoacrylate glue was used to close a gap between the edge of the coverslip and the skull. After the glue dried, the junction between the coverslip and the skull was strengthened by dental cement.

After the end of the surgery an analgesic dose of carprofen (5 µg/g BW, Pfizer, Berlin, Germany) was administered subcutaneously for 3 days and an antibiotic baytril (1:100 v/v, Bayer, Leverkusen, Germany) was added to drinking water for 10 days. The clarity of the window was examined 4 weeks after the surgery. After this time period mice that passed quality control were injected with lentivirus encoding fluorescent Ca^{2+} sensor Twitch-2B under the ubiquitin promoter into the RMS of the left and right hemispheres.

Virus injection into the RMS

Mice were anesthetized with i.p. injections of ketamine/xylazine (80/4 µg/g of BW) and fixed in the stereotaxic device (Stoelting, Wood Dale, IL, USA) by ear bars. Bepanthen (Bayer, Germany) was applied on the eyes of the mouse to prevent dehydration. Lidocaine 2% (AstraZeneca, Wedel, Germany) was applied subcutaneously for local analgesia. During the surgery depth of the anaesthesia was monitored by toe pinch and when necessary additional

ketamine/xylazine (40/2 µg/g of BW) was injected. Temperature of the mouse was monitored with rectal temperature probe connected to the digital thermometer. During the surgery, and until full recovery the mouse was kept on a heating plate having a temperature 37-38 °C.

Skin overlying the skull was removed to free the injection sites and craniometric points: lambda and bregma. Thereafter small holes in the skull were made above the injection sites using a microdrill. Injection sites had the following coordinates: 3 mm anterior and 0.82 lateral from the bregma and 2.9 mm ventral from the surface of the brain. Approximately 1 µl lentivirus encoding fluorescent Ca^{2+} sensor Twitch-2B under the ubiquitin promoter was injected into the left and right hemispheres.

After injections were done and injection pipette was removed from the brain, the screw housing was fixed with dental cement to the skull between the ears to be used for the head fixation during subsequent imaging sessions. Additional dental cement was used to cover exposed parts of the skull. After the end of the surgery an analgesic dose of carprofen (5 µg/g BW, Pfizer, Berlin, Germany) was administered subcutaneously for 3 days. 3 days after injection mice were subjected to a training period of 5 days allowing mice to be used to the imaging system.

Training of the mice

At the 3rd day post-injection (DPI) the experimentator was putting his hand inside the cage without further movements letting the mouse to familiarize itself with it and to go on the palm. When mouse was on palm animal was gently removed from the cage leaving it on the palm, in order to make the mouse to be used to the hands. After 5 minutes mouse was returned back to the cage. This procedure was

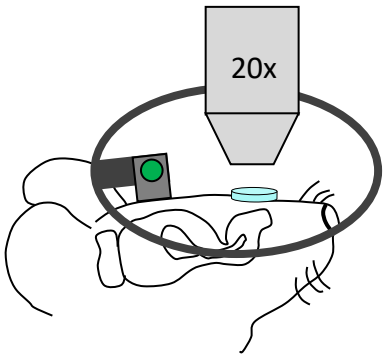

Figure 4. Schematic representation of the fixation system

done several times during 4th day post-injection.

At the 4th day post-injection mouse was taken in arms and transferred to the microscope system. Animal was allowed to move freely under the microscope to explore new environment and to get used to it.

At the 5th day post-injection mouse was taken in arms and transferred to the microscope system and fixed with the screw in the fixation ring under the objective for 20 minutes (Figure 4). After this time mouse was returned back to the cage. This procedure was repeated twice a day.

At the 6th and 7th day post-injection mouse was fixed under the objective for 40 and 60 minutes respectively, twice in a day.

Starting from 8th day post-injection (DPI 8), two-photon in-vivo Ca^{2+} imaging in awake state was performed immediately after the fixation of the animal, followed by the imaging under the isoflurane-induced anaesthesia.

Two-photon in-vivo Ca^{2+} imaging

Two-photon excitation laser scanning microscopy is special type of fluorescence microscopy where focused laser beam is used to excite fluorescent dyes that were previously delivered to the cells of interest. Wavelengths of the photons that are used in two-photon excitation laser scanning microscopy are in the deep red or near infra-red parts of the spectrum. These photons penetrate tissue better than their visible wavelength counterparts but due to the long wavelength they have relatively low energy (see the Planck's equation above). Because of this, energy of each single photon used in two-photon excitation laser scanning microscopy is not enough to excite fluorophores. Only being precisely focused in space and time, two low-energy photons cooperate to excite a single molecule of a fluorescent dye in the cells of interest.

$$E = \frac{hc}{\lambda}$$

Planck's equation. E – energy of the photon; *h* - Planck's constant; *c* – speed of light; λ - wavelength of the photon

Efficiency of the excitation provided by the focused laser beam is highest at the focal plane of the objective and drops off quadratically with distance above and below [Svoboda and Yasuda, 2006]. Thus, two-photon excitation laser scanning microscopy allows selective visualization of only those cells that are located in the focal plane of the objective. By moving the focal plane, it is possible to excite fluorophores in cells that are located in the living tissue at different depths. In the present research, in-vivo study we studied adult-born JGNs located at the depth ranging from 10 µm to approximately 180 µm below the surface of the olfactory bulb.

Being excited by a couple of low-energy photons, fluorophores, located in the cell of interest start to emit photons. The emitted photons have different energy and therefore also the wavelength compared to the excitation light photons [Benninger and Piston 2013]. The emitted photons are collected by the same objective that is used for excitation and guided to the photomultiplier tubes (PMT) that serve as photodetectors. Subsequent processing of the signal acquired by the PMT leads to a build-up of a digital image that represents distribution of emission intensity over the field of view of the objective.

Because two-photon excitation laser scanning microscopy provides a digital image of the fluorescently labelled specimen, this method usually, in a simplified manner, is called two-photon imaging.

A set of successive images acquired varying the focal plane from up to down with step size of 1-2 µm can be used for reconstruction of a 3D morphology of a given cell and revealing spatial relationships between several labelled cells located in the volume of the tissue scanned by two-photon imaging. Whereas sequence of images acquired from the same focal plane over a given period of time can be used for studying dynamic intracellular processes such as spontaneous and sensory evoked Ca^{2+} signals, in case if given cell is labelled with a fluorescent dye that is sensitive to the intracellular concentration of Ca^{2+}.

Fluorescent Ca^{2+} indicator Twitch-2B was delivered to immature adult-born neurons via injection of lentivirus, encoding this construct, into the RMS. Twitch-2B is comprised of two fluorescent proteins: mCerulean3 and cpVenus^{CD}

[Thestrup et al. 2014]. mCerulean3 and cpVenus^{CD} are linked by a Ca^{2+}-binding region. Being excited in the absence of Ca^{2+} both fluorophores emit photons independently from each other. But upon binding of calcium to a linking region the distance between mCerulean3 and cpVenus^{CD} becomes shorter. This enables Förster resonance energy transfer (FRET) [Förster V.T., 1948]. FRET refers to the process of energy transfer from an excited donor fluorophore to an acceptor fluorophore [Svoboda and Yasuda, 2006]. FRET decreases fluorescence intensity of the donor (mCerulean3) and increases fluorescence intensity of the acceptor (cpVenus^{CD}) (Figures 5, 6). Efficiency of this process can be measured as a ***ratio*** of emission intensity of cpVenus^{CD} to emission intensity of mCerulean3.

Due to low number of calcium binding sites, the efficiency of FRET in Twitch-2B is dependent on free cytosolic concentration of Ca^{2+} in almost linear manner [Thestrup et al. 2014]. Thus, dynamics of free cytosolic concentration of Ca^{2+} is reflected in corresponding dynamics of *cpVenus^{CD}/mCerulean3 ratio*.

During in-vivo two-photon imaging, brightness of both fluorophores in different cells may be altered due to different expression levels of Twitch-2B, different laser intensities used for excitation of cells located at different depth and due to the movement of the animal. Fortunately, ratiometric measurements provide normalization for these artefacts, making it possible to compare results acquired from different cells [Thestrup et al. 2014].

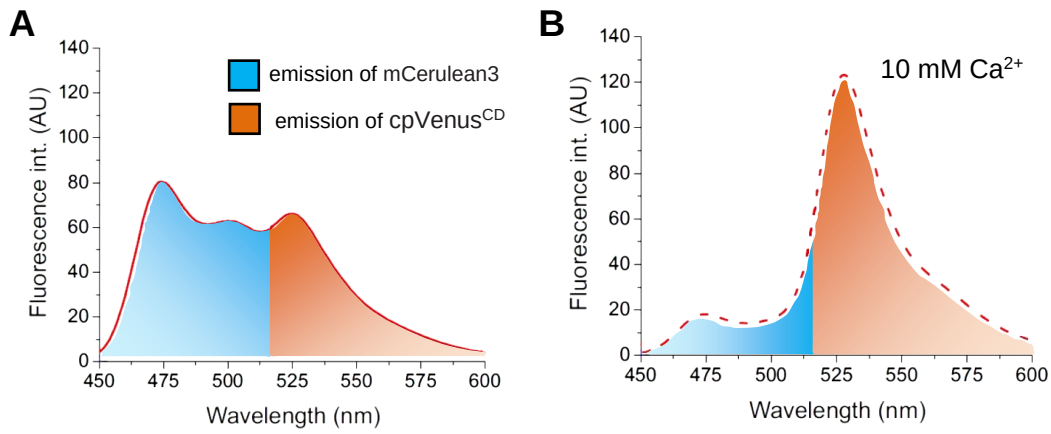

Figure 5. Schematic illustration of emission spectra of equimolar amounts of purified Twitch-2B. (**A**) basal condition (**B**) calcium saturation. (modified from Thestrup et al. 2014)

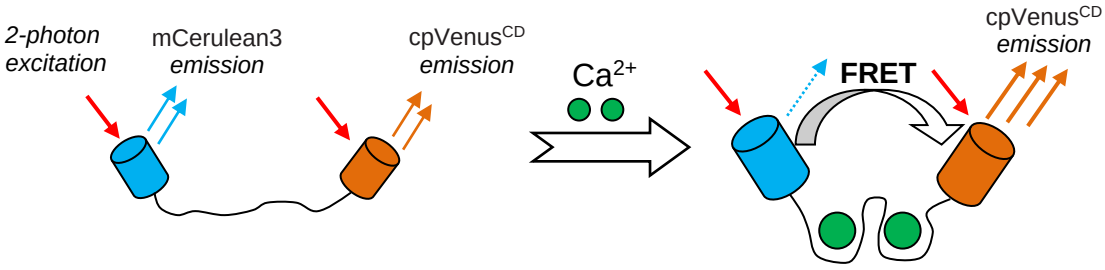

Figure 6. Schematic illustration of FRET-based fluorescent Ca^{2+} sensor Twitch-2B

In-vivo two-photon imaging of spontaneous and odorant-evoked calcium transients through implanted cranial window

Two-photon imaging started 8 or 9 days after injection of lentivirus encoding fluorescent calcium sensor Twitch-2B into the rostral migratory stream of the mouse. Animal was fixed to the x-y table under the Zeiss 20x water immersion objective. Imaging was done using a customized two-photon microscope based on Olympus FV-1000 system (Olympus, Tokyo, Japan) and MaiTai Deep See Laser (Spectra Physics, Mountain View, CA) with wavelength of excitation light 890 nm.

First, a part of the glomerular layer of the olfactory bulb, accessible through an implanted cranial window was scanned from the surface into the depth of approximately 180 µm in order to identify adult-born JGNs labelled with Twitch-2B. After this, focal plane of the objective was adjusted to the level of the soma of a given Twitch-$2B^+$ adult-born JGN.

To study dynamics of intracellular calcium concentration of adult-born JGNs in awake state, for each cell we performed in-vivo time-lapse two-photon imaging session for a period of approximately 2 minutes. After awake imaging was done, animal was anesthetized with isoflurane (1-0.4% in O_2; CP-Pharma, Germany) and same cells were imaged again. During imaging under anaesthesia mouse was kept on a heating plate, temperature of the animal was

monitored and maintained at the level of 36-37°C. Respiratory rate was monitored and maintained at the level 100-140 breaths per minute. Bepanthen (Bayer, Germany) was applied on the eyes of the mouse to prevent dehydration.

It was technically challenging to acquire stable in-vivo recordings, especially in awake state of the animal. Due to this reason measurements were often limited to only one 2 minutes-long imaging session for a given neuron in awake state and usually two such imaging sessions under anaesthesia.

Next day, awake in-vivo time-lapse imaging of Twitch-2B^{+} adult-born JGNs was done again as described above. After these measurements, the mouse was anesthetized with intraperitoneal injection of a 3 component anaesthesia, consisting of a mixture of midazolam (5 mg/kg BW), medetomidine (0.5 mg/kg BW), and fentanyl (0.05 mg/kg BW). Under these conditions, two-photon imaging of odorant-evoked calcium signals was performed for the same immature adult-born JGNs that were measured for spontaneous calcium signals in awake stake. Mouse was kept on a heating plate, temperature of the animal was monitored and maintained at the level of 36-37°C. Breathing rate was monitored. Bepanthen (Bayer, Germany) was applied on the eyes of the mouse to prevent dehydration. Odorants were applied through a custom-made flow dilution olfactometer positioned in front of the mouse's snout [Vucinić et al. 2006]. Olfactory sensory neurons making mono- and polysynaptic connections with JGNs including adult-born cells were stimulated with a mixture of three odorants (isoamyl acetate, 2-hexanone and ethyl tiglate; 0.6% of saturated vapour each). The duration of an odorant pulse was 4 s, time of corresponding imaging session approximately 20 seconds. All the odorants were purchased from Sigma-Aldrich.

To study developmental aspects of spontaneous calcium signalling in adult-born JGNs, next sessions of time-lapse in-vivo calcium imaging in awake state were performed as described above at later time points – DPI 20-22.

Data analysis

As mentioned above, Twitch-2B consists of two fluorescent proteins mCerulean3 and cpVenus^{CD} that are linked by a short calcium-binding region. These fluorophores have different spectrum of emission wavelengths and due to this, emission of each fluorophore can be detected separately in the following way. Photons emitted by mCerulean3 or cpVenus^{CD} during two-photon imaging session, were collected by the objective and guided to a dichroic mirror (515 nm long pass). This mirror allows photons emitted by one fluorophore (cpVenus^{CD}) to pass through to the photomultiplier tube 2 (PMT2) while reflecting photons emitted by the second fluorophore (mCerulean3) to the PMT1.

After the processing signals from PMT1 and PMT2, each scan of the cell, labelled with Twitch-2B, results in simultaneous acquisition of matched pair of images. Image acquired from PMT1 originates from emission of mCerulean3, whereas image acquired from PMT2 originates from emission of cpVenus^{CD}. During one time-lapse imaging session over the period of approximately 2 minutes we acquired approximately 720 pairs of matched images where emission intensity of each fluorophore is represented by the brightness intensity of the image of the cell acquired from corresponding PMT.

The images were analysed with ImageJ software. First, time-series of images were splitted into two stacks, each representing data acquired from corresponding PMT. Then, for each image in both stacks the mean brightness intensity of the cell and the mean brightness intensity of the background were calculated. These data were processed further with IgorPro software. Brightness intensity of the background was subtracted from the values of brightness intensity of the cell. Resulting values acquired from two matched stacks of images were plotted against corresponding acquisition time to visualize dynamics of cpVenus^{CD} and mCerulean3. After this, **ratio** of cpVenus^{CD}/mCerulean3 was calculated and plotted against time. Resulting trace of the ratio of cpVenus^{CD}/mCerulean3 reflects temporal dynamics of the intracellular calcium concentration in adult-born JGN (Figure 7).

Noise was filtered using boxcar smooth algorithm that was applied twice for each trace of the ratio (Figure 8). Boxcar or sliding average smoothing replaces each value of the ratio in the trace with the average of it and its 2 neighbours.

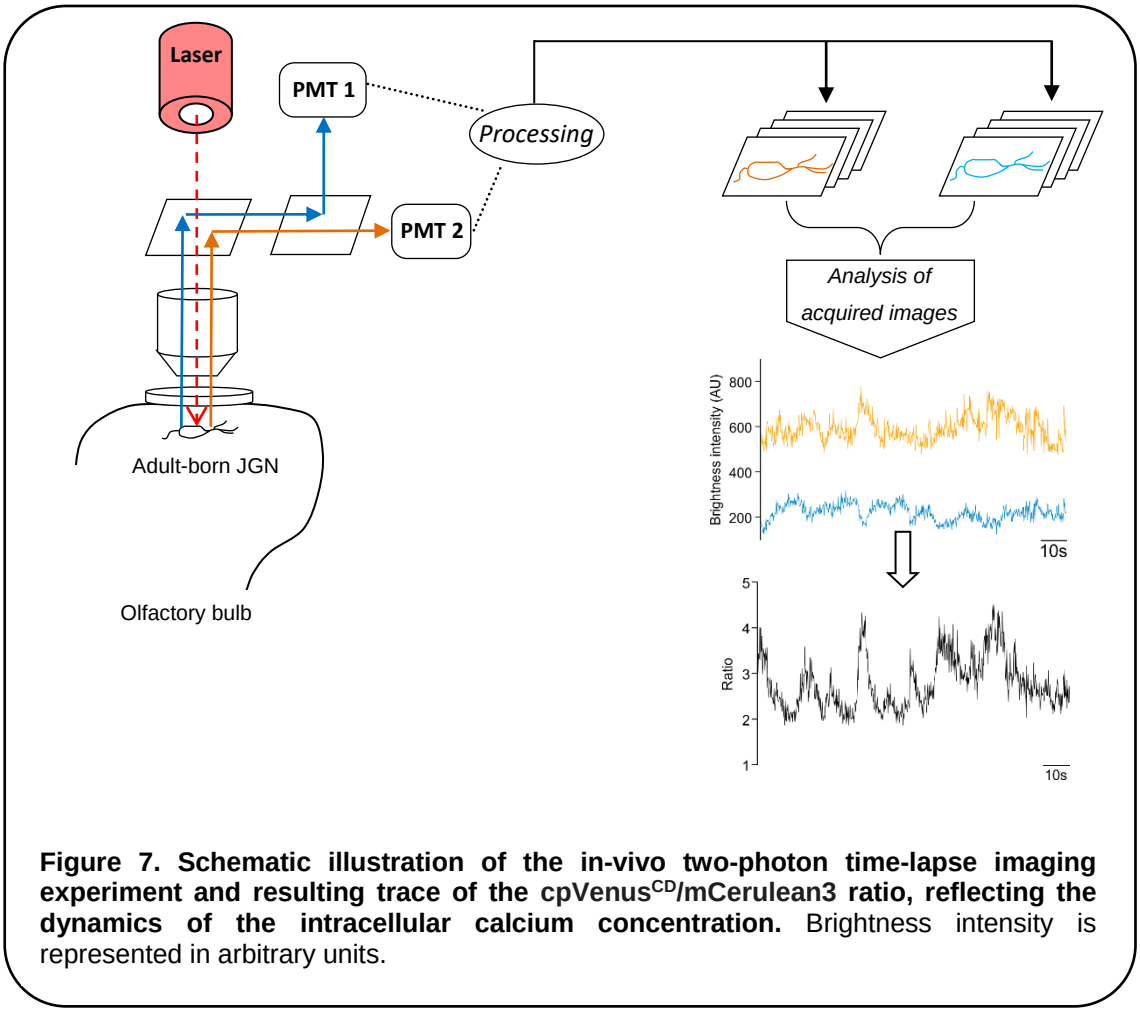

Figure 7. Schematic illustration of the in-vivo two-photon time-lapse imaging experiment and resulting trace of the cpVenus^{CD}/mCerulean3 ratio, reflecting the dynamics of the intracellular calcium concentration. Brightness intensity is represented in arbitrary units.

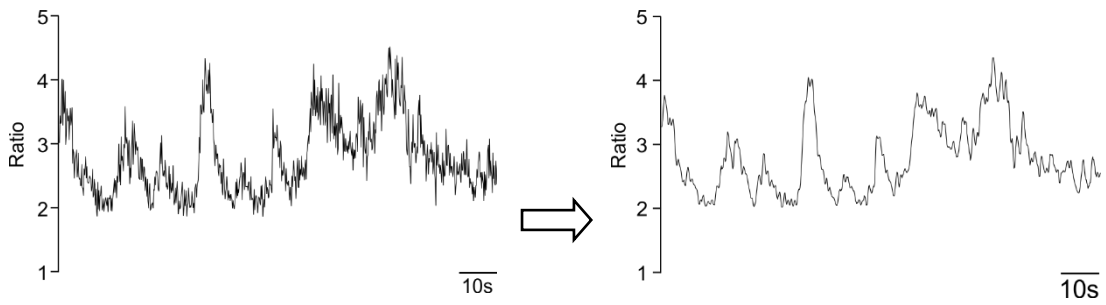

Figure 8. Illustration of the noise filtering with box smooth algorithm.

Acute In-vivo two-photon imaging

Acute two-photon in-vivo imaging was performed in separate group of mice (without previous implantation of the window) at 10-12 days post injection of lentivirus encoding Twitch-2B into the rostral migratory stream. Mouse was anesthetized using isoflurane (1-1.5% in O_2; CP-Pharma, Germany) and kept on a heating plate (37°C) to maintain temperature of the body. Bepanthen (Bayer, Germany) was applied on the eyes of the mouse to prevent dehydration. Local anaesthetic lidocaine 2% was injected under the skin located above the olfactory bulb. Skin was removed to expose the skull. Custom-made recording chamber with a hole in the middle was glued to the skull with cyanoacrylic glue in such way that opening in the centre of the chamber was positioned above the olfactory bulb. The skull over the olfactory bulb was thinned under the microscope using a microdrill. A small craniotomy (approximately $1mm^2$) was performed above the olfactory bulb using a thin (30G) syringe needle. The mouse was transferred to the two-photon microscope. Head-attached chamber was fixed on X-Y table under the Zeiss 20x water immersion objective. Mouse was kept on a heating plate and was supplied with 0.6-1% isoflurane in pure moistened oxygen. Temperature of the body of the animal was maintained at 36-37°C. Respiratory rate was monitored and maintained at the level 100-140 breaths per minute. Exposed olfactory bulb was covered with a gel freshly prepared from agarose dissolved in standard extracellular solution.

The recording chamber was perfused with standard extracellular solution of following composition: 125 mM NaCl, 4.5 mM KCl, 26 mM $NaHCO_3$, 1.25 mM NaH_2PO_4, 2 mM $CaCl_2$, 1 mM $MgCl_2$ and 20 mM glucose, pH 7.4, bubbled continuously with 95% O2 and 5% CO2. Temperature of standard extracellular solution was maintained at the level of 36-37°C (Figure 9).

In-vivo two-photon time-lapse imaging of Twitch-$2B^+$ adult-born JGNs was performed as described above. Those adult-born JGNs that showed calcium signals in 3 successive time-lapse imaging sessions were chosen for further 2 or 3 successive time-lapse imaging sessions that were performed 40

minutes after 2 µM of TTX was added to the standard extracellular solution. Time-series of images acquired during acute in-vivo two-photon imaging sessions were analysed as described above.

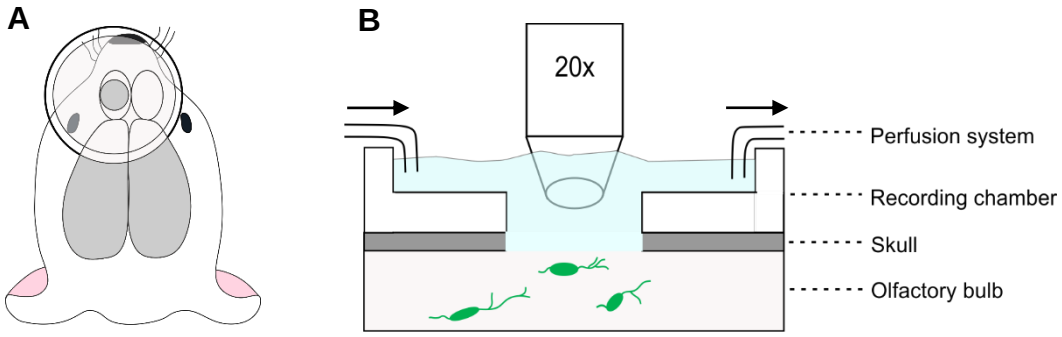

Figure 9. Schematic illustration of the recording chamber. (A) View of the chamber mounted on the scull of the mouse. **(B)** Side view of the chamber during In-vivo two-photon imaging. Arrows indicate direction of the flow of standard extracellular solution.

Parameters used to characterize spontaneous calcium transients in adult-born JGNs

Addition of 2 µM tetrodotoxin (TTX) to the standard extracellular solution blocked spontaneous calcium signals in all spontaneously active immature adult-born JGNs studied in acute experiments (see results, Figure 15). Thus, it was considered that traces of the cpVenus^{CD}/mCerulean3 ratio, measured under these conditions, reflect baseline level of intracellular calcium concentration in adult-born JGNs.

Maximal values of cpVenus^{CD}/mCerulean3 ratio, measured under 2 µM TTX were used to empirically define the threshold separating the active and silent periods in the cellular activity pattern. **Maximal ratio** was calculated as average of the highest value on the filtered trace and 4 neighbouring data-points (Figure 10). Maximal values of cpVenus^{CD}/mCerulean3 ratio, measured under 2 µM of TTX varied between 1.76 and 1.92 (n=6 cells, 4 mice).

Value of the ratio = 2.4 that is obviously higher than maximal ratio measured in-vivo under TTX was chosen as a threshold for detection of time periods when the cell is found in an active state (Figure 11).

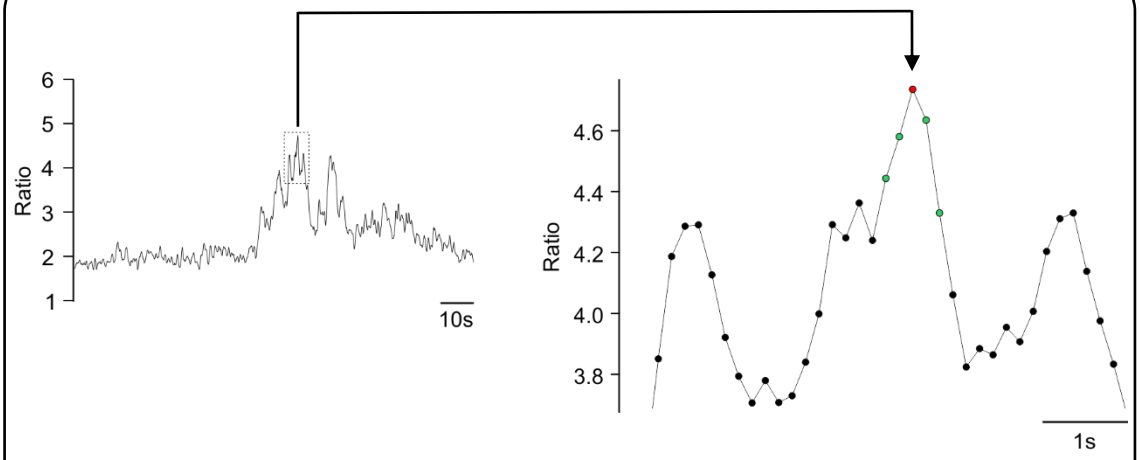

Figure 10. Illustration of the cpVenus^{CD}/mCerulean3 ratio trace with data-points (in red and green) used for calculation of the maximal ratio.

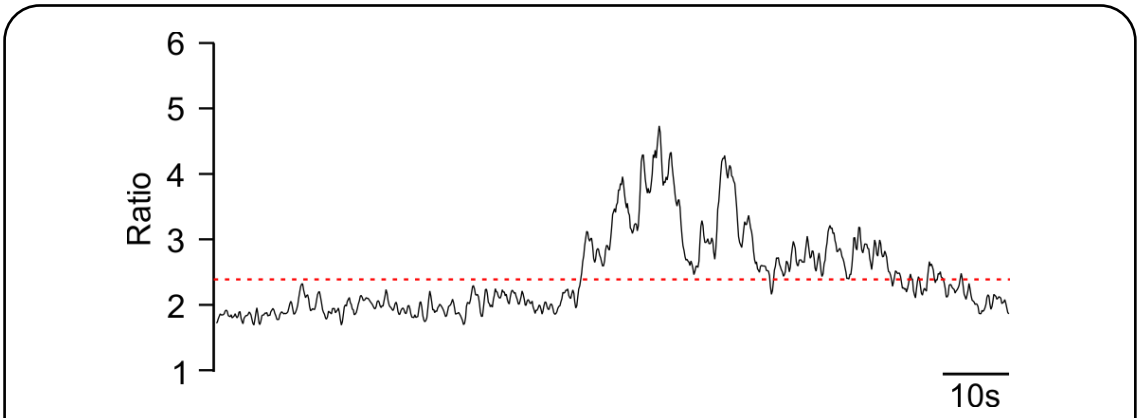

Figure 11. Illustration of the cpVenus^{CD}/mCerulean3 ratio trace with the threshold level for signal detection (ratio=2.4).

In order to characterize the properties of spontaneous calcium transients, following parameters were measured from each ratio trace, showing an elevation above the value of 2.4:

- the maximal ratio
- the fraction of the time spent in the active state
- the normalized area under the curve during the active time period

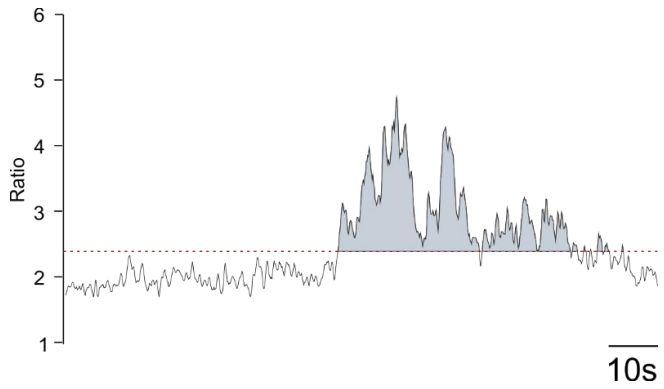

Figure 12. Illustration of the shape created by the cpVenus^{CD}/mCerulean3 ratio trace and the level of the ratio=2.4 that is used to calculate normalized area under the curve of the signal.

In those cases when for a given adult-born neuron imaging sessions were performed twice or 3 times under the same condition (awake/anesthetized), fraction of the time spent in active state and area under the curve of the signal were calculated for each trace and averaged to acquire resulting values. For calculation of the maximal ratio the highest observed value was chosen.

In a few cases (6 out of 44 cells studied in awake and under isoflurane) only part of spontaneous calcium transient was recorded during a period of 2 minutes (Figure 13). In 5 of these traces duration of recorded signal was equal or more than 20% of the total time of a given imaging session. And in one of these traces the duration of recorded signal was 8% of the total time of the imaging session.

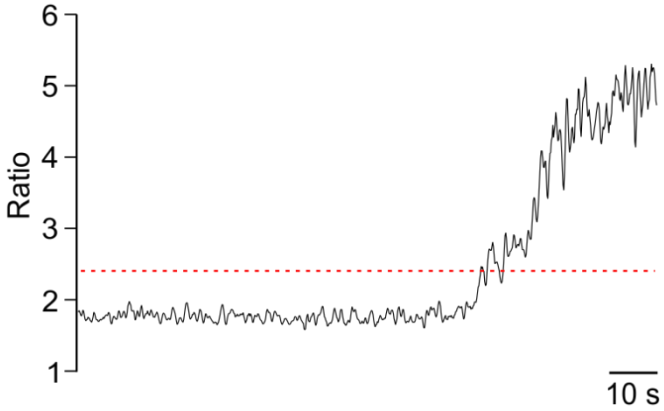

Figure 13. Illustration of the partly recorded spontaneous calcium transient.

Statistical analysis

Statistical analyses were done using the software available on the Vassar Stats web site (http://vassarstats.net/). For multiple measurements within the same data set Wilcoxon Signed-Rank test was used. Mann-Whitney test was used for comparisons between the two independent data sets. For comparison of the fractions of silent, intermittently active, and constantly active adult-born JGNs between different data sets (DPI 8-11 and DPI 20-22) Chi-square test was used. The difference was considered statistically significant at $p < 0.05$.

Immunohistochemistry

For immunohistochemical study of the expression of neurochemical markers by adult-born JGNs, mice were injected into the rostral migratory stream with a retrovirus encoding enhanced green fluorescent protein (eGFP) under the control of chicken β-actin promoter, as described above. Mice were sacrificed at DPI 9 and DPI 20-24. After decapitation brains were removed and fixed with 4% formaldehyde in phosphate-buffered saline (PBS) for 24 h at 4°C.

After this, brains were put in PBS containing 25% sucrose (overnight, at 4°C), and then embedded in Tissue Tek (Sakura, Zoeterwoude, The Netherlands) and freezed at -80°C.

Labelling with antibodies was performed at room temperature on free-floating horizontal slices with thickness of approximately 30 µm. Sections were treated with a blocking solution (5% normal donkey serum and 1% Triton-X 100 in PBS) for 1 h to prevent non-specific background staining. Then slices were exposed overnight to primary antibodies diluted in blocking solution. After this, sections were rinsed three times for 10 min in PBS and incubated in darkness for 2 h with secondary antibodies that were diluted 1:1000 (in PBS +2% bovine serum albumin). Then sections were washed in PBS three times, positioned on glass slides (Langenbrink, Emmendingen, Germany) and mounted in Vectashield Mounting Medium (Vector Laboratories, Burlingame, CA).

For the multiple staining, for example against eGFP and one or two specific neurochemical markers, we used following primary antibodies:

- goat or rabbit anti-eGFP (Rockland, 1:2500 or 1:1500):
- rabbit polyclonal antibody against Doublecortin (Dcx, Abcam, 1:2000)
- mouse monoclonal antibody against Polysialic acid–neural cell adhesion molecule (PSA-NCAM, Chemicon, 1:1500)
- sheep polyclonal antibody against tyrosine hydroxylase (TH, Millipore, 1:2000)
- mouse monoclonal antibody against calretinin (Swant, 1:2000)
- rabbit polyclonal antibody against calbindin (Swant, 1:4000)

The secondary antibodies:

- Donkey-anti-goat or anti-rabbit IgG-conjugated Alexa Fluor 488 (Molecular Probes, 1:1000),
- Donkey-anti-rabbit, anti-mouse or anti-sheep IgG-conjugated Alexa Fluor 594 (1:1000)
- Donkey-anti-mouse IgG conjugated Alexa Fluor 680 (1:1000)

All secondary antibodies were purchased from Molecular Probes (Molecular Probes, Eugene, OR).

After labelling, slices were imaged using Nikon 40x water immersion objective mounted on the Olympus Fluoview 300 laser scanning microscope operating with the MaiTai laser (Spectra Physics, Mountain View, CA). Alexa Fluor 488 and Alexa Fluor 594 were excited simultaneously at a laser wavelength 800 nm and their fluorescence was splitted with a dichroic mirror 630 nm long pass (LP). This dichroic mirror guided photons emitted by Alexa Fluor 488 to PMT1 and photons emitted by Alexa Fluor 594 to PMT2. Photons coming to PMT1 were additionally filtered with a 536/40 band pass filter allowing only photons with wavelength 516-556 nm to go through. Photons coming to PMT2 were additionally filtered with a 568 LP filter.

Alexa Fluor 680 and Alexa Fluor 488 were excited simultaneously at a laser wavelength 900 nm and their fluorescence was splitted with a dichroic mirror 670 nm long pass (LP). This dichroic mirror guided photons emitted by Alexa Fluor 488 to PMT1 and photons emitted by Alexa Fluor 680 to PMT2. Photons coming to PMT2 were additionally filtered with a 568 LP filter.

Acquired matched pairs of images visualizing $eGFP^+$ adult-born JGNs and cells positive for a given neurochemical marker were acquired and analysed using Olympus FluoView10-ASW and ImageJ software.

Results

Spontaneous Ca^{2+} transients in immature adult-born JGNs

To test for the presence of spontaneous Ca^{2+} transients in immature adult-born JGNs, the cells were labelled with the fluorescent ratiometric calcium indicator Twitch-2B and studied in-vivo by means of time-lapse two-photon laser scanning microscopy. After the viral injection into the RMS, first labelled immature neurons started to arrive into the glomerular layer of the olfactory bulb at day post injection (DPI) 5 or DPI 6 but the number of newcomers at this time was very low [Kovalchuk et al. 2015]. In order to have enough cells to study, two-photon time-lapse imaging started between DPI 8 and DPI 11. Results acquired in chronic experiments with previously implanted cranial window over the olfactory bulb showed that immature adult-born JGNs exhibit spontaneous calcium transients under isoflurane-induced anaesthesia (Figure 14).

To test whether spontaneous calcium signals in immature adult-born JGNs are sensitive to voltage-gated Na^+ channel blocker tetrodotoxin (TTX), in-vivo two-photon time-lapse imaging was performed through acute craniotomy over the olfactory bulb under isoflurane-induced anaesthesia at DPI 10-12. Those adult-born JGNs, which in several successive imaging sessions showed spontaneous calcium transients under control conditions (in standard extracellular solution), were chosen for further time-lapse imaging sessions, which started 40 minutes after 2 µM TTX was added to the extracellular solution. Results of these experiments showed that 2 µM TTX block spontaneous calcium transients in immature adult-born JGNs (Figure 15). Maximal values of $cpVenus^{CD}$/mCerulean3 ratio, measured in control condition varied between 4.53 and 6.1 (n=6 cells, 4 mice), while maximal values of $cpVenus^{CD}$/mCerulean3 ratio recorded from the same adult-born JGNs under 2 µM of TTX varied between 1.76 and 1.92. Thus, parts of recording traces with $cpVenus^{CD}$/mCerulean3 ratio<2 were considered as silent time periods during which cells were not spiking. The $cpVenus^{CD}$/mCerulean3 ratio>2.4 was

considered to reflect an active state, whereas the ratio range between 2 and 2.4 was ascribed to an uncertain state.

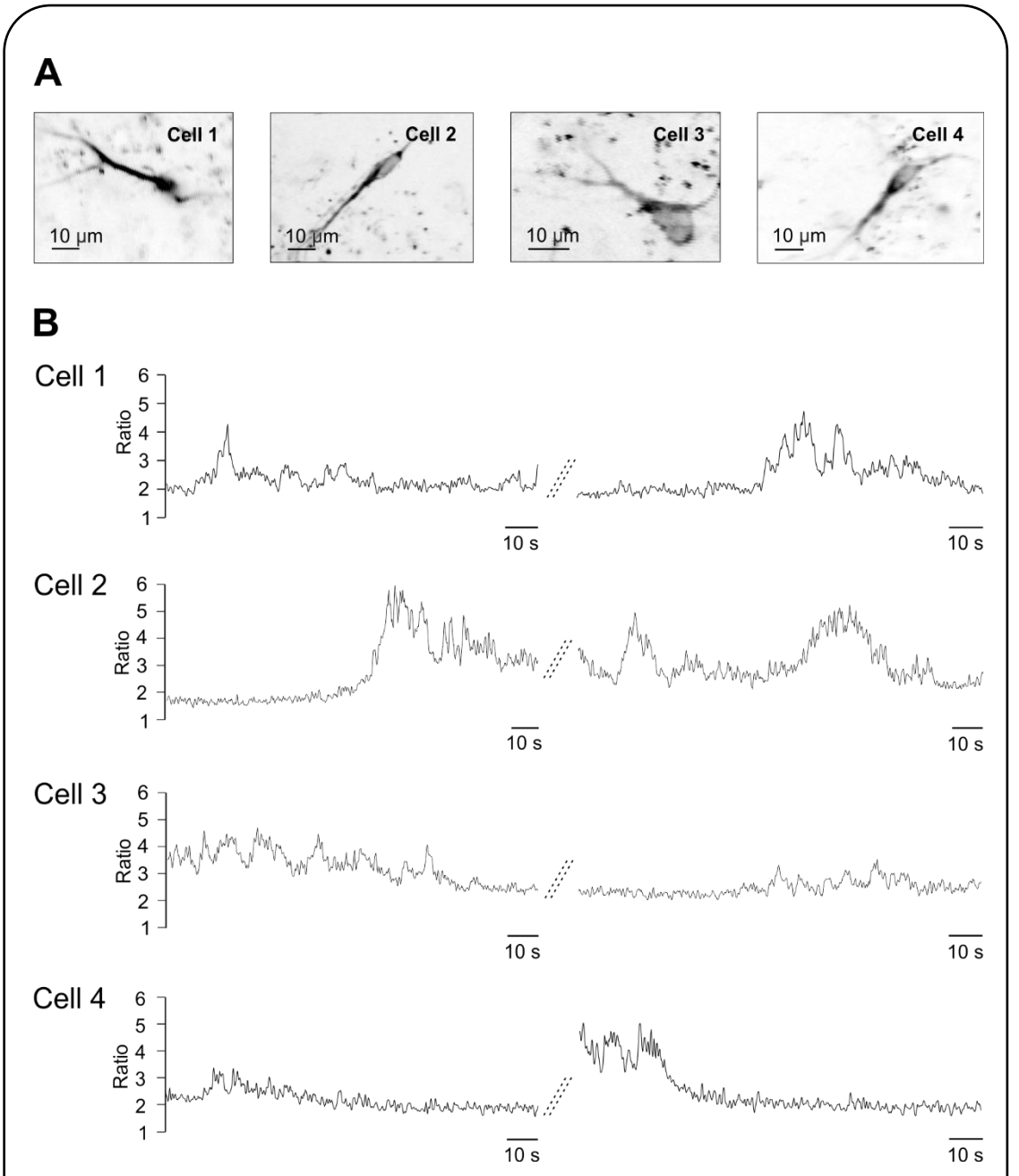

Figure 14. Spontaneous Ca^{2+} transients in immature adult-born juxtaglomerular neurons (JGNs) DPI 8-11. (**A**) In-vivo images of adult-born JGNs labelled with the fluorescent ratiometric Ca^{2+} sensor Twitch-2B. (**B**) Spontaneous Ca^{2+} transients recorded from cells 1-4 under isoflurane anaesthesia.

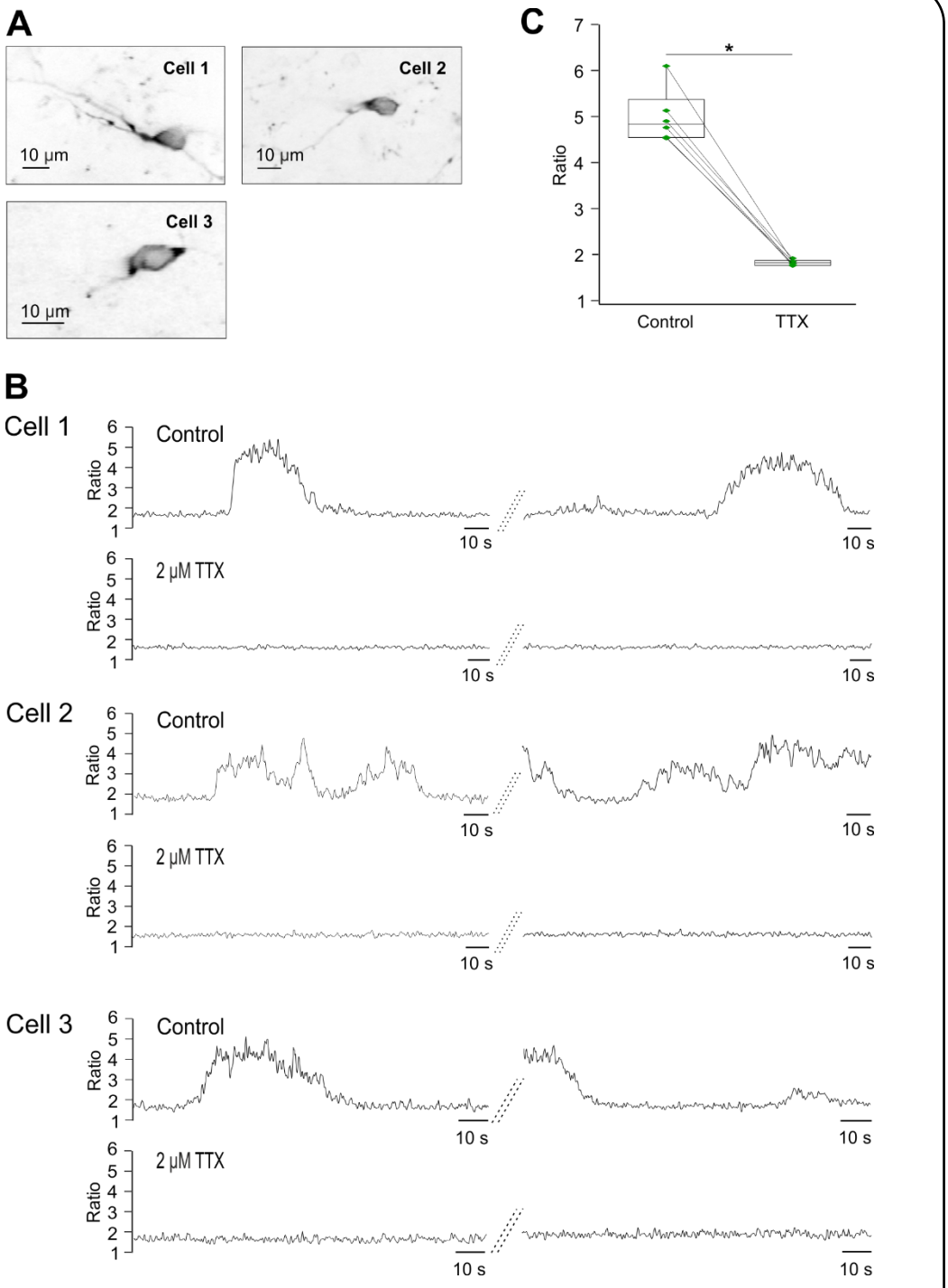

Figure 15. Effect of the TTX on spontaneous Ca^{2+} transients in adult-born JGNs DPI 10-12. (**A**) In-vivo images of Twitch-2B^{+} adult-born JGNs. (**B**) Spontaneous Ca^{2+} transients recorded from cells 1-3 under isoflurane anaesthesia in normal Ringer solution as control condition and subsequently in Ringer solution with addition of 2 µM TTX. (**C**) Box plots illustrating the distributions of maximal ratios of signals measured from the same Twitch2B^{+} adult-born JGNs (DPI 10-12) in control and under TTX (n=6 cells, 4 mice). Asterisk denotes a significant difference between the data obtained in control and in the presence of 2 µM TTX (p=0.05, Wilcoxon signed-rank test).

It has to be mentioned, that in acute experiments only a few adult-born JGNs showed spontaneous calcium transients under control conditions, whereas when in-vivo two-photon imaging was performed through previously implanted window, most of the studied immature adult-born JGNs showed spontaneous Ca^{2+} transients. I hypothesized that this happened due to acute trauma induced by the craniotomy.

To verify the observation that majority of immature adult-born JGNs show spontaneous calcium transients, we performed paired in-vivo time-lapse imaging in awake state and under isoflurane, through the chronic cranial window previously implanted over the olfactory bulbs.

In some cases, it was difficult to target the same neurons in awake state and under the anaesthesia because immature adult-born neurons can change their morphology during experiment. Due to this reason number of all immature (DPI 8-11) adult-born JGNs studied in awake state (n=55 cells, 5 mice) was higher than number of neurons that were studied in both conditions (n=48 cells, 5 mice). For analyses shown in Figure 16 I chose only paired measurements, in which the same adult-born JGNs were reliably identified in awake state and under anaesthesia, (n=48 cells, 5 mice).

Results of paired measurements from the same adult-born JGNs in awake state and under anaesthesia (Figure 16) confirmed that majority of analysed immature adult-born JGNs showed spontaneous Ca^{2+} transients. Although one mouse showed only 18,18% of spontaneously active adult-born JGNs under anaesthesia, when same cells were measured in awake state, 72.73% of them showed spontaneous calcium transients. Other 4 mice showed high percentage of spontaneously active immature adult-born JGNs in both conditions. Still, in 4 out of 5 mice there was a trend towards an anaesthesia-induced decrease in the fraction of spontaneously active cells, which, however, did not reach the statistic significance ($p>0.05$, Wilcoxon signed-rank test). Thus, spontaneous calcium transients can be considered as characteristic feature of immature adult-born JGNs in awake state and under anaesthesia. However, patterns of spontaneous calcium transients often changed between the two conditions. Even when measured from the same cells, the fraction of

time spent by an adult-born JGNs in an active state tended to be higher in awake state of the mouse, while maximal values of cpVenus^{CD}/mCerulean3 ratio seemed to be higher under isoflurane-induced anaesthesia. So, I hypothesized that isoflurane-induced anaesthesia can change properties of spontaneous calcium signals in immature adult-born JGNs.

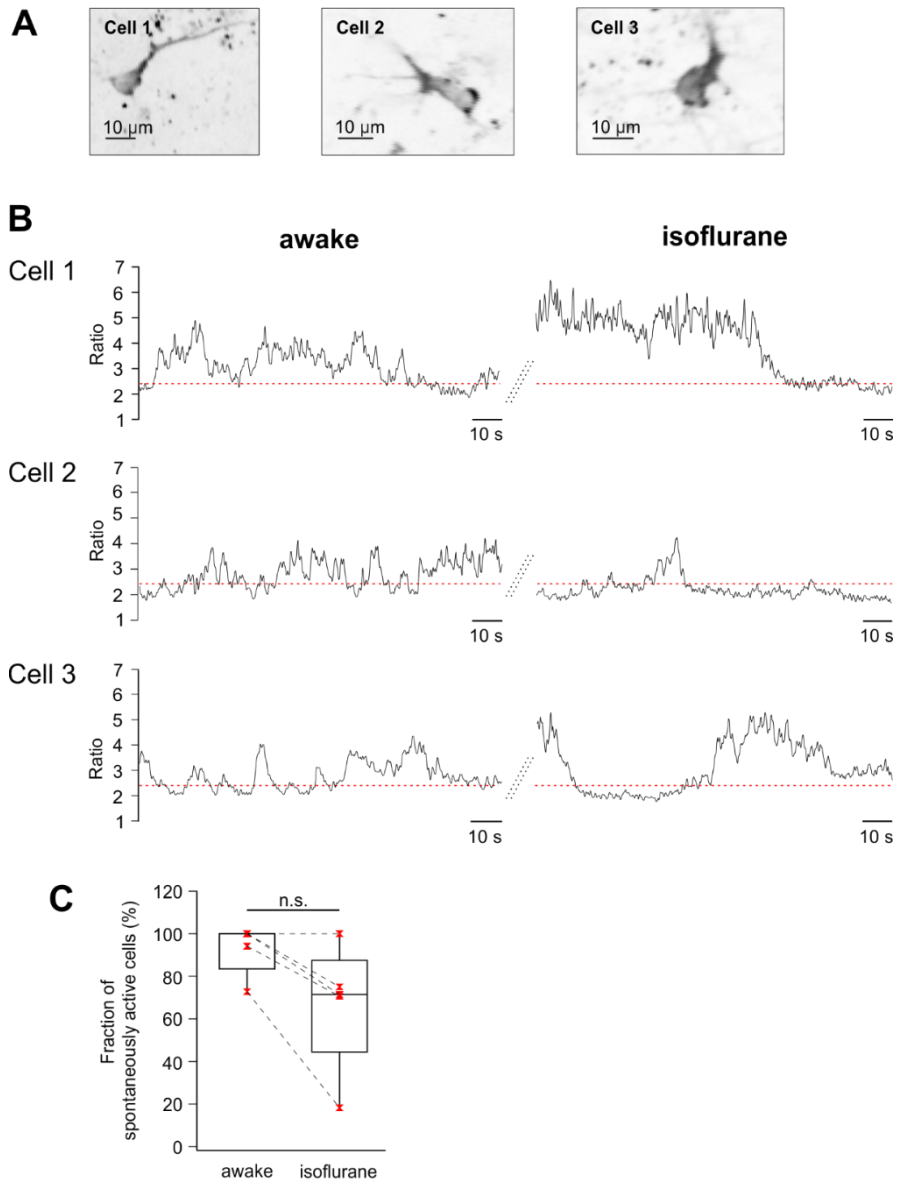

Figure 16. Spontaneous Ca^{2+} transients in adult-born DPI 8-11 JGNs measured under anaesthesia and in awake state. (**A**) In-vivo images of adult-born JGNs labelled with the fluorescent ratiometric Ca^{2+} sensor Twitch-2B. (**B**) Spontaneous Ca^{2+} transients recorded from cells 1-3 in awake state and under anaesthesia. Red lines denote level of the ratio=2.4. (**C**) Box plots illustrating distributions of the percentage (pro mouse) of spontaneously active adult-born JGNs. Same cells were measured in awake state and under isoflurane (n=48 cells, 5 mice). The two distributions are not significantly different (p>0.05, Wilcoxon signed-rank test).

Properties of spontaneous calcium transients in immature adult-born JGNs in awake state and under the isoflurane-induced anaesthesia.

Different types of calcium transients lead to different effects on neuronal differentiation during embryonic development [Rosenberg and Spitzer 2011]. So, it was reasonable to ask whether isoflurane-induced anaesthesia significantly changed the patterns of spontaneous calcium transients in immature adult-born JGNs. To address this question following parameters were measured from the cpVenus^{CD}/mCerulean3 ratio traces recorded from same neurons in awake state and under isoflurane-induced anaesthesia (see methods, pages 28-30):

- the maximal ratio
- the fraction of time spent in the active state
- the normalized area under the curve during the active time period

It should be noted that for calculation of these parameters I chose only those adult-born JGNs that were active in awake state and subsequently measured under anaesthesia (n=44 cells, 5 mice).

All of the mentioned above parameters showed a cell-to-cell variability both in awake state as well as under the anaesthesia (Figures 18A, 19A, 20A). However, it was not possible to compare statistically overall distributions of the values of a given parameter measured in awake state and under the anaesthesia for significance of the difference between them because all the measurements were performed as paired recordings. Therefore, we compared the median values of a given parameter between the two experimental conditions.

Distribution of 5 medians of a given parameter calculated from each of 5 mice in awake state was compared with corresponding distribution of 5 medians acquired from these mice under the isoflurane-induced anaesthesia.

As it is evident from Figures 18B, 19B, 20B, for all three parameters which were chosen to characterize traces of spontaneous calcium signals there

was no significant difference between values measured in awake state and under the isoflurane-induced anaesthesia.

Thus, initial hypothesis that isoflurane-induced anaesthesia may cause significant changes in the properties of spontaneous calcium signals in adult-born JGNs was disproved.

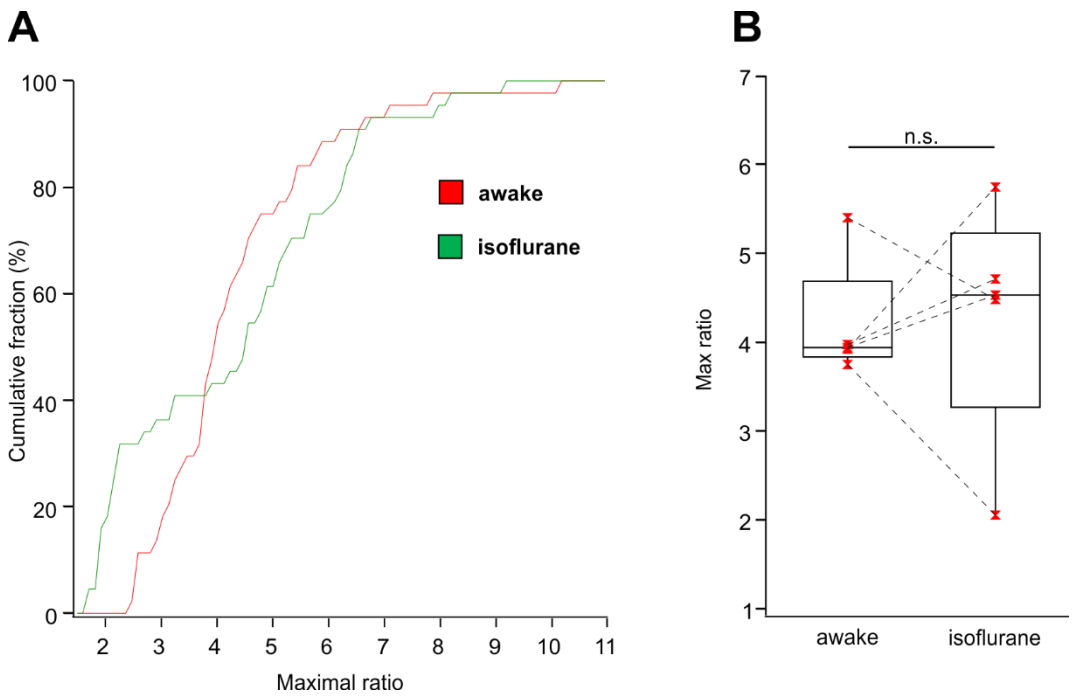

Figure 17. Maximal ratio of spontaneous Ca^{2+} transients of adult-born JGNs (DPI 8-11) in awake state vs. isoflurane-induced anaesthesia. (**A**) The cumulative probability histograms showing the overall distribution of the values of maximal ratio of spontaneous Ca^{2+} transients of cells measured under both experimental conditions (n=44 cells, 5 mice). (**B**) Box plots illustrating distributions of 5 medians calculated from the groups of cells from each mouse in awake state and under anaesthesia. The two distributions are not significantly different ($p>0.05$, Wilcoxon signed-rank test).

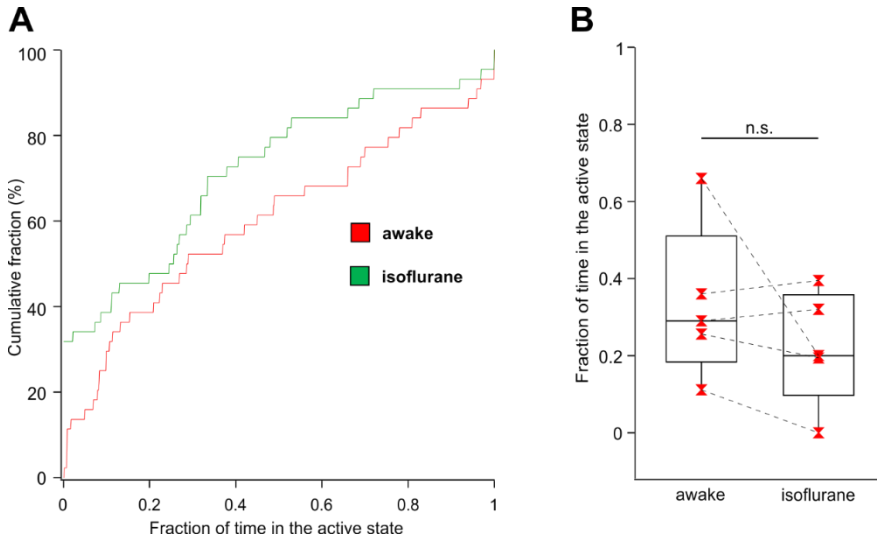

Figure 18. Fraction of time spent by adult-born JGNs (DPI 8-11) in the active state in awake state vs. isoflurane-induced anaesthesia. (**A**) The cumulative probability histograms showing the overall distribution of the values for fraction of time spent in the active state of cells measured under both experimental conditions. (n=44 cells, 5 mice). (**B**) Box plots illustrating distributions of 5 medians calculated from the groups of cells from each mouse in awake state and under anesthesia. The two distributions are not significantly different (p>0.05, Wilcoxon signed-rank test).

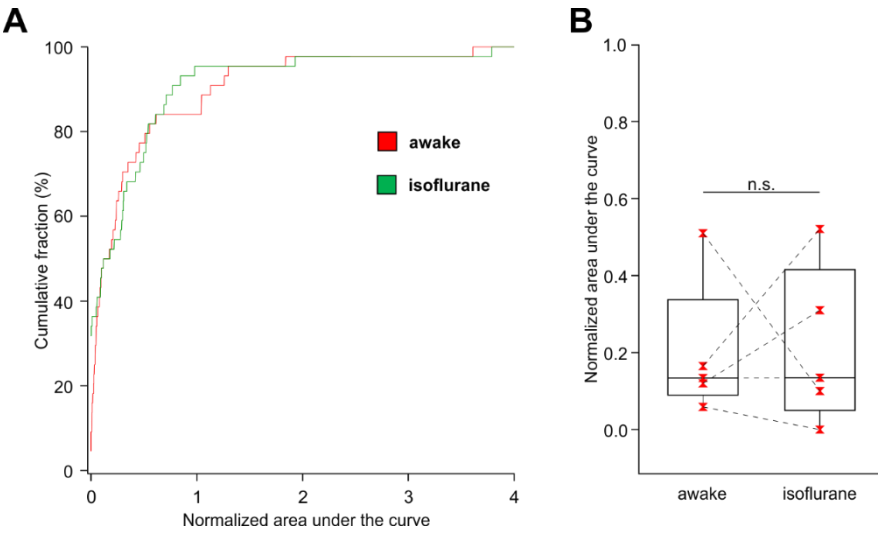

Figure 19. Normalized area under the curve for adult-born JGNs (DPI 8-11) in awake state vs. isoflurane-induced anaesthesia. (**A**) The cumulative probability histograms showing the overall distribution of the values for normalized area under the curve of cells measured under both experimental conditions. Same cells were measured in awake state and under isoflurane (n=44 cells, 5 mice). (**B**) Box plots illustrating distributions of 5 medians calculated from the groups of cells from each mouse in awake state and under anaesthesia. The two distributions are not significantly different (p>0.05, Wilcoxon signed-rank test).

Odorant-evoked responses in spontaneously active immature adult-born JGNs

Upon arrival into the glomerular layer of the olfactory bulb, immature adult-born JGNs start to integrate into the mature neuronal circuit, acquiring the odorant-responsiveness. To reveal whether spontaneous activity of immature adult-born JGNs ontogenetically precedes the odorant-evoked activity, we performed in-vivo two-photon imaging of dynamics of intracellular calcium concentration during presentation of the odorants in front of the mouse's snout. Axons of olfactory sensory neurons make mono- and polysynaptic connections with dendrites of JGNs inside the glomerular layer of the olfactory bulb. Thus, presentation of the odorants to olfactory sensory neurons represents physiologically-relevant stimuli to adult-born JGNs.

Odorant-evoked calcium signals were studied in 5 mice. In 1 mouse from this group odorant-evoked calcium signals were studied during the same day when the paired in-vivo imaging in awake state and under isoflurane-induced anaesthesia was performed. In 4 other mice odorant-evoked calcium signals were studied on another day. Because of this reason the time window of experiments with odorant presentation was shifted from DPI 8-11 to DPI 9-11.

Odorant-evoked calcium signals were studied in those cells that were spontaneously active in awake state. Due to active migration of immature adult-born JGNs inside of the glomerular layer [Liang et al. 2016], usually it was not possible to recognize the same adult-born JGNs measured on two different days even over a period of only 24 hours. So, in order to identify spontaneously-active immature adult-born JGNs again, 2 minutes long imaging sessions in awake state were performed once more on the day of odorant-presentation. After identification of spontaneously active adult-born JGNs, the mouse was anesthetized with intraperitoneal injection of 3 component anaesthesia (see Methods, page 24) and in-vivo two-photon imaging of odorant-evoked calcium transients was performed. Mixture of 3 odorants was presented in a brief 4-second-long pulse during a 14-second-long two-photon imaging session. It

seemed that 3 component anaesthesia reduced spontaneous activity in immature adult-born JGNs, however there were not enough data to test this suggestion statistically.

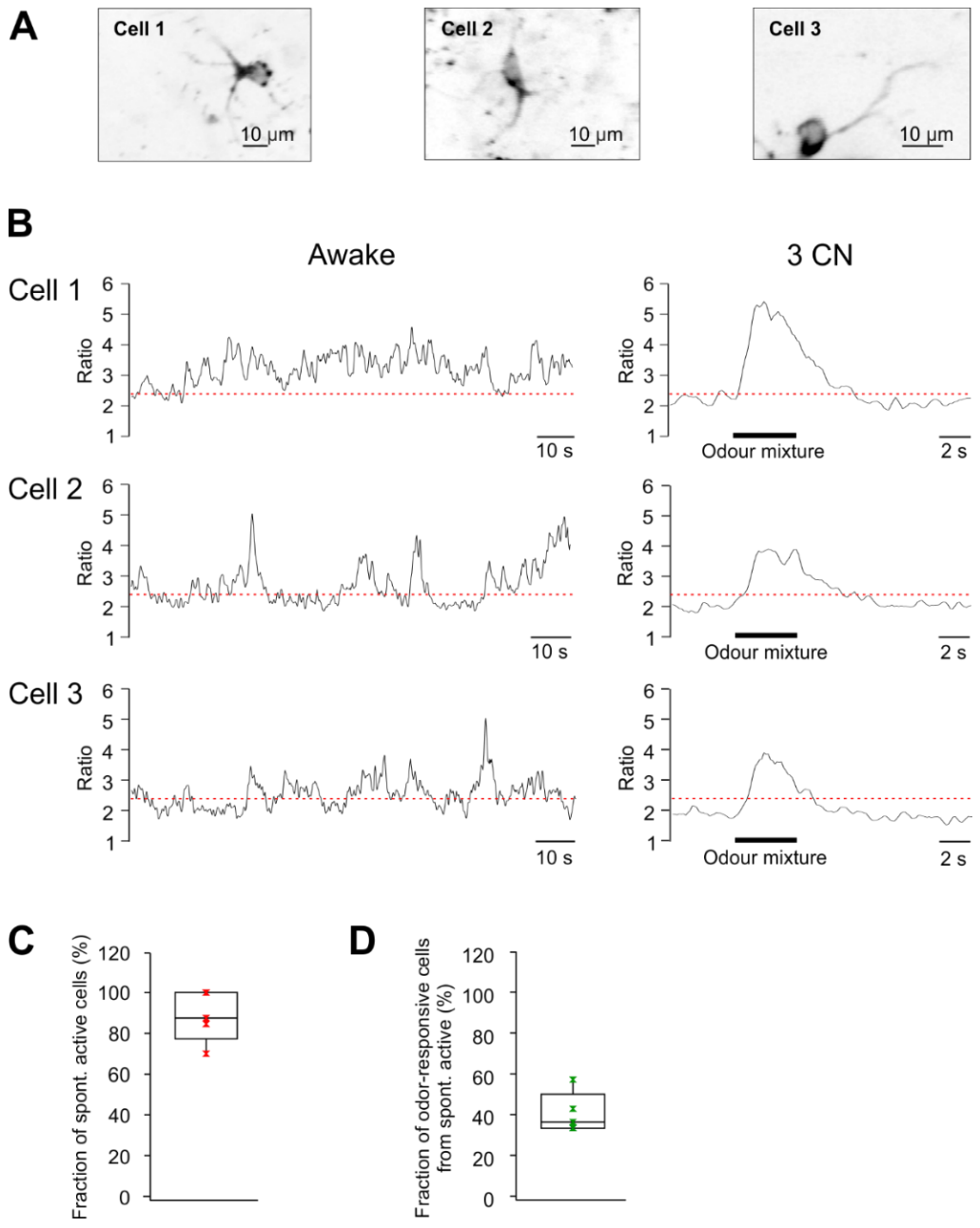

Figure 20. Odorant-evoked responses in spontaneously active immature (DPI 9-11) adult-born JGNs. (**A**) In-vivo images of Twitch-2B^{+} adult-born JGNs. (**B**) Spontaneous Ca^{2+} transients recorded from cells 1-3 in awake state and odorant-evoked Ca^{2+} transients recorded from these cells under 3-component anaesthesia. Red lines denote level of the ratio=2.4. (**C**) Box plot illustrating distribution of the percentage (per mouse) of spontaneously active adult-born JGNs at DPI 9-11 (n=46 cells, 5 mice). (**D**) Box plot illustrating distribution of the percentage (per mouse) of odorant-responsive cells from those that were spontaneously active in awake state (n=40 cells, 5 mice).

Figure 20B illustrates traces of spontaneous calcium signals and odorant-evoked calcium transients recorded from same cells in awake and under 3-component anaesthesia respectively. The percentage of spontaneously active adult-born JGNs in awake state that was calculated for time-window DPI 9-11 was similar to what was revealed for DPI 8-11 (Figure 20C). In each of 5 mice that were studied in these experiments a fraction of adult-born JGNs, which showed spontaneous calcium signals in awake stake were odorant-responsive (Figure 21D). Percentage of odorant-responsive immature adult-born JGNs per mouse was ranging between 33.33% and 57.14% (Median value of percentage of odorant-responsive immature adult-born JGNs from spontaneously active ones 36.36% with interquartile range IQR=16.67).

Since not all immature adult-born JGNs which were spontaneously active in the awake state showed odorant-evoked calcium transients, I hypothesized that there may be a significant difference between the properties of spontaneous calcium transients of odorant-responsive versus odorant non-responsive cells. To address this question and to reveal whether properties of spontaneous calcium transients can be predictive for odorant-responsiveness of immature adult-born JGNs, the maximal ratio, the fraction of time spent in the active state, and the normalized area under the curve of spontaneous calcium transients of odorant-responsive JGNs were compared with properties of spontaneous calcium transients of odorant non-responsive JGNs.

Values of mentioned above parameters acquired from all spontaneously active JGNs studied for odorant-responsiveness (n=40 cells, 5 mice) showed similar distribution in both groups – the one of odorant-responsive as well as odorant non-responsive JGNs (Figure 21A, 22A, 23A).

For the group of odorant-responsive and odorant non-responsive adult-born JGNs were acquired different numbers of cells from each of five mice. For the group of adult-born JGNs spontaneously active in awake state and odorant-responsive under the 3-component anaesthesia, we identified n=4, 3, 2, 3, 4 cells (n=5 mice) For the group of adult-born JGNs spontaneously active in awake state and odorant non-responsive under 3-component anaesthesia n=3, 6, 4, 4, 7 cells (n=5 mice) were identified. As for comparison of parameters of

spontaneous calcium transients between awake state and isoflurane-induced anaesthesia described above, medians were calculated from a distribution of the values of a given parameter acquired from each of 5 mice. Distribution of 5 medians of a given parameter calculated for the group of odorant-responsive JGNs were compared with corresponding distribution of 5 medians calculated for the group of odorant non-responsive JGNs. Results are presented in Figures 21, 22, 23 showed that there was no statistically significant difference in the properties of spontaneous Ca^{2+} transients in awake mice between odorant-responsive and odorant non-responsive immature adult-born JGNs.

Thus, substantial fraction of immature adult-born JGNs, which are spontaneously active in awake state, are able to show odorant-evoked responses, indicating the overlap in spontaneous and sensory-driven types of activity in the development of immature adult-born JGNs. Furthermore, the properties of spontaneous Ca^{2+} transients cannot be predictive for odorant-responsiveness of a given immature adult-born JGN.

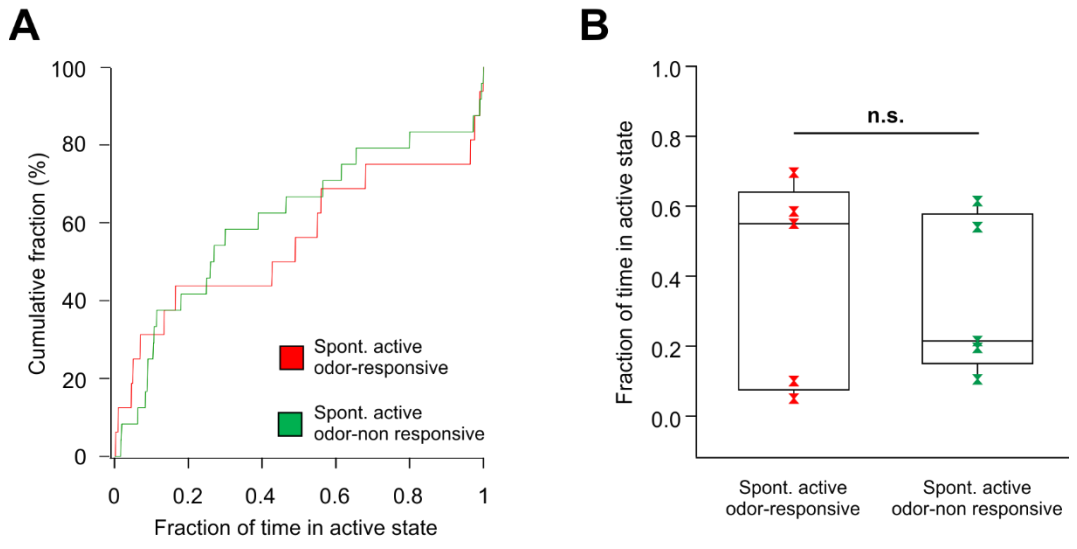

Figure 21. Comparison of the fraction of time spent in the active state by odorant-responsive and odorant non-responsive adult-born JGNs (DPI 9-11). (A) The cumulative probability histograms showing the overall distribution of the values for fraction of time spent in the active state for odorant-responsive (red) vs. odorant non-responsive (green) immature adult-born JGNs (n=40 cells, 5 mice). (**B**) Box plots illustrating distributions of 5 medians calculated from odorant-responsive and odorant non-responsive groups of cells from each mouse. The two distributions are not significantly different (p=1, Mann-Whitney test).

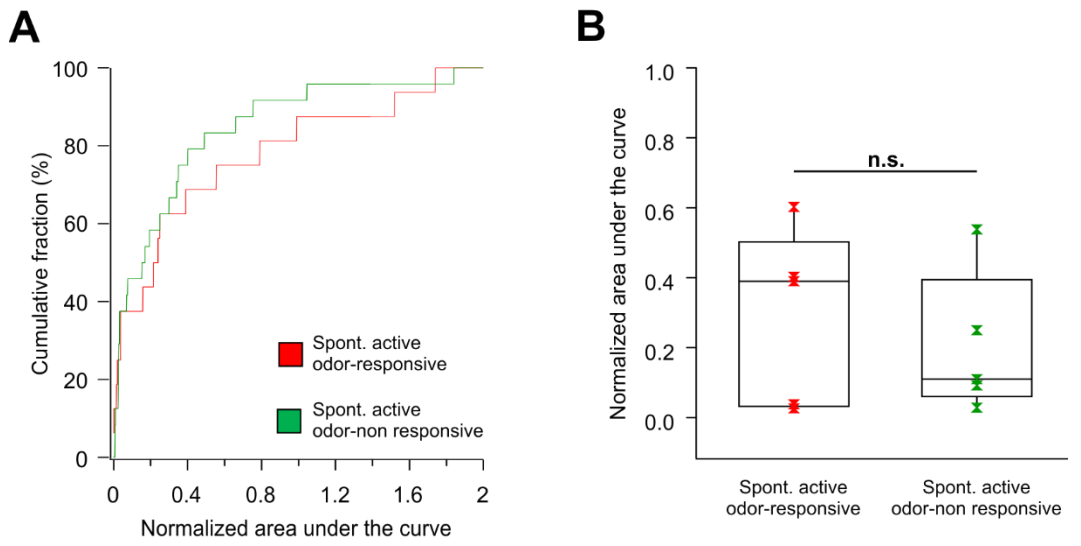

Figure 22. Comparison of the normalized area under the curve of odorant-responsive and odorant non-responsive adult-born JGNs (DPI 9-11). (A) The cumulative probability histograms showing the overall distribution of the values for normalized area under the curve for odorant-responsive (red) and odorant non-responsive (green) immature adult-born JGNs (n=40 cells, 5 mice). (**B**) Box plots illustrating distributions of 5 medians calculated from odorant-responsive and odorant non-responsive groups of cells from each mouse. The two distributions are not significantly different (p=0.83, Mann-Whitney test).

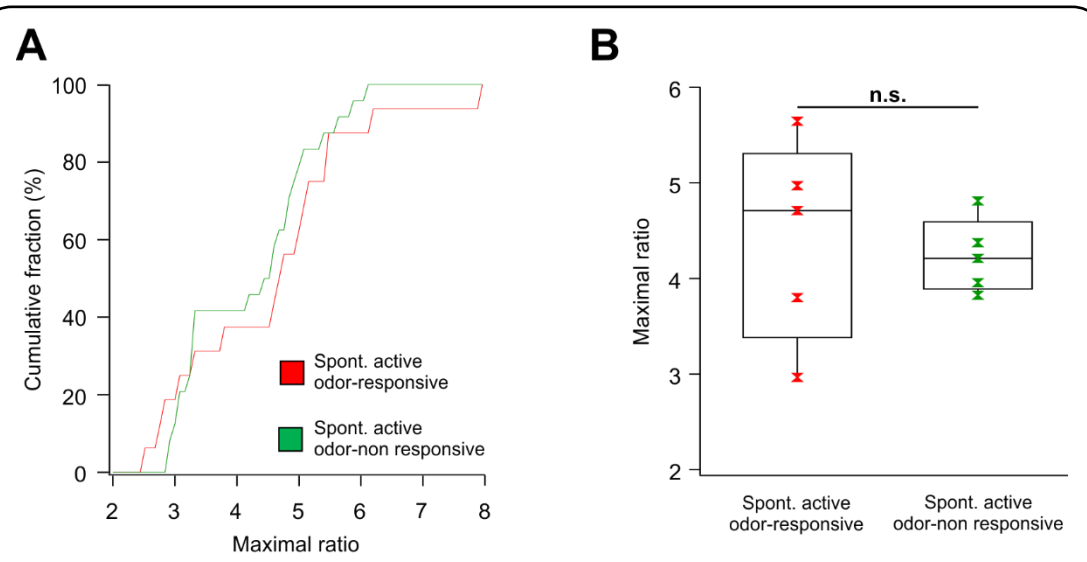

Figure 23. Comparison of the maximal ratio of spontaneous Ca^{2+} transients of odorant-responsive and odorant non-responsive adult-born JGNs (DPI 9-11). (**A**) The cumulative probability histograms showing the overall distribution of the values for maximal ratio of spontaneous Ca^{2+} transients for odorant-responsive (red) and odorant non-responsive (green) immature adult-born JGNs (n=40 cells, 5 mice). (**B**) Box plots illustrating distributions of 5 medians calculated from odorant-responsive and odorant non-responsive groups of cells from each mouse. The two distributions are not significantly different (p=0.83, Mann-Whitney test).

Neurochemical properties of immature adult-born JGNs

To reveal neurochemical profile of immature adult-born JGNs and to study how it changes during integration of adult-born JGNs into the mature neuronal circuit, expression of neurochemical markers was studied in these cells at 2 time-points:

- Soon after their arrival into the glomerular layer of the olfactory bulb (DPI 9), when the majority of adult-born JGNs show active migration [Kovalchuk et al. 2015; Liang et al. 2016].
- At the time when most of adult-born JGNs stop their migration inside of the glomerular layer of the olfactory bulb [Liang et al. 2016]

Following neurochemical markers were analysed by means of immunohistochemistry and two-photon imaging of fixed, approximately 30 µm-thick slices of the olfactory bulb (Figure 24A):

- Polysialylated neuronal cell adhesion molecule (PSA-NCAM) – marker of immature migrating neurons.
- Doublecortin (Dcx) – marker of immature migrating neurons, microtubule-associated protein that is involved in translocation of the nucleus during migration.
- Tyrosine hydroxylase (TH) – rate-limiting enzyme for synthesis of dopamine.
- Calbindin – a calcium-binding protein.
- Calretinin – a calcium binding protein.

JGNs, positive for TH, calbindin and calretinin represents predominantly non-overlapping subpopulations [P. Panzanelli et al. 2007]. Almost all immature adult-born JGNs at DPI 9 were positive for PSA-NCAM and Dcx, while expression of another markers that were studied at this age, was very limited (Figure 24B). The percentage of adult-born JGNs that were positive for TH, calbindin and calretinin at DPI 20-24 compared to DPI 9 (Figure 24C). These results were published [Kovalchuk et al. 2015].

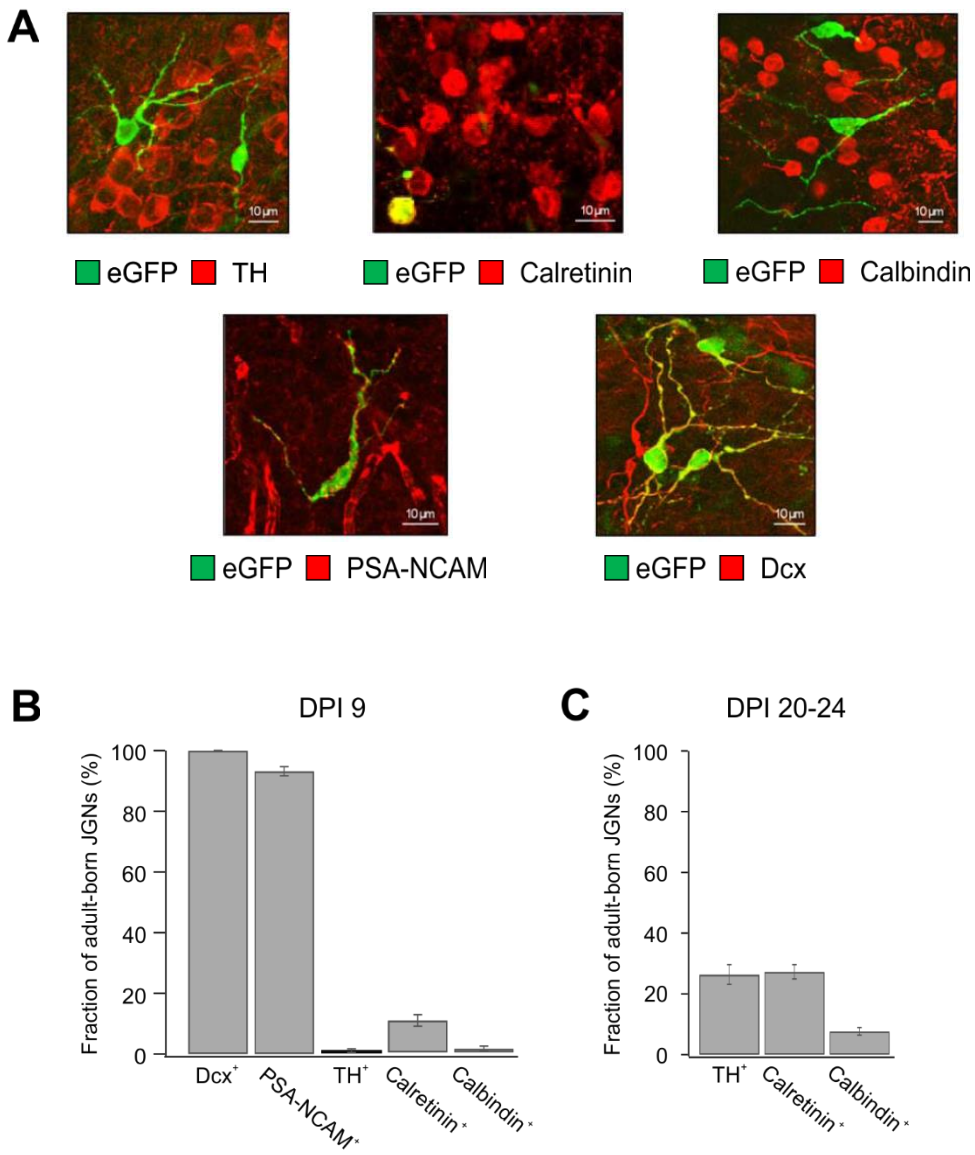

Figure 24. Neurochemical marker expression by adult-born JGNs at DPI 9 and DPI 20-24. (Modified from Kovalchuk et al. 2015). (**A**) Images of eGFP$^+$ adult-born JGNs (green) labelled with antibodies against different neurochemical markers (red), as indicated. (**B**) Summary graph illustrating the fraction of adult-born JGNs, positive for a given marker at DPI 9. Results are presented as mean ± standard error of mean (SEM). TH and calretinin n=156 cells, 5 mice; calbindin n=151 cells, 5 mice; Dcx n=83 cells, 4 mice; PSA-NCAM n=109 cells, 4 mice. (**C**) Summary graph illustrating the fraction of adult-born JGNs, positive for given marker at DPI 20-24. TH and calretinin n=126 cells, 4 mice; calbindin n=118 cells, 4 mice.

Developmental aspects of spontaneous Ca^{2+} transients in adult-born JGNs

To reveal developmental aspects of spontaneous calcium transients in adult-born JGNs, in-vivo two-photon time-lapse imaging was performed in awake state for approximately 2 minutes at DPI 20-22. In every mouse (n=74 cells, 5 mice) tested in these experiments, the majority of adult-born JGNs showed spontaneous calcium transients (Figure 25).

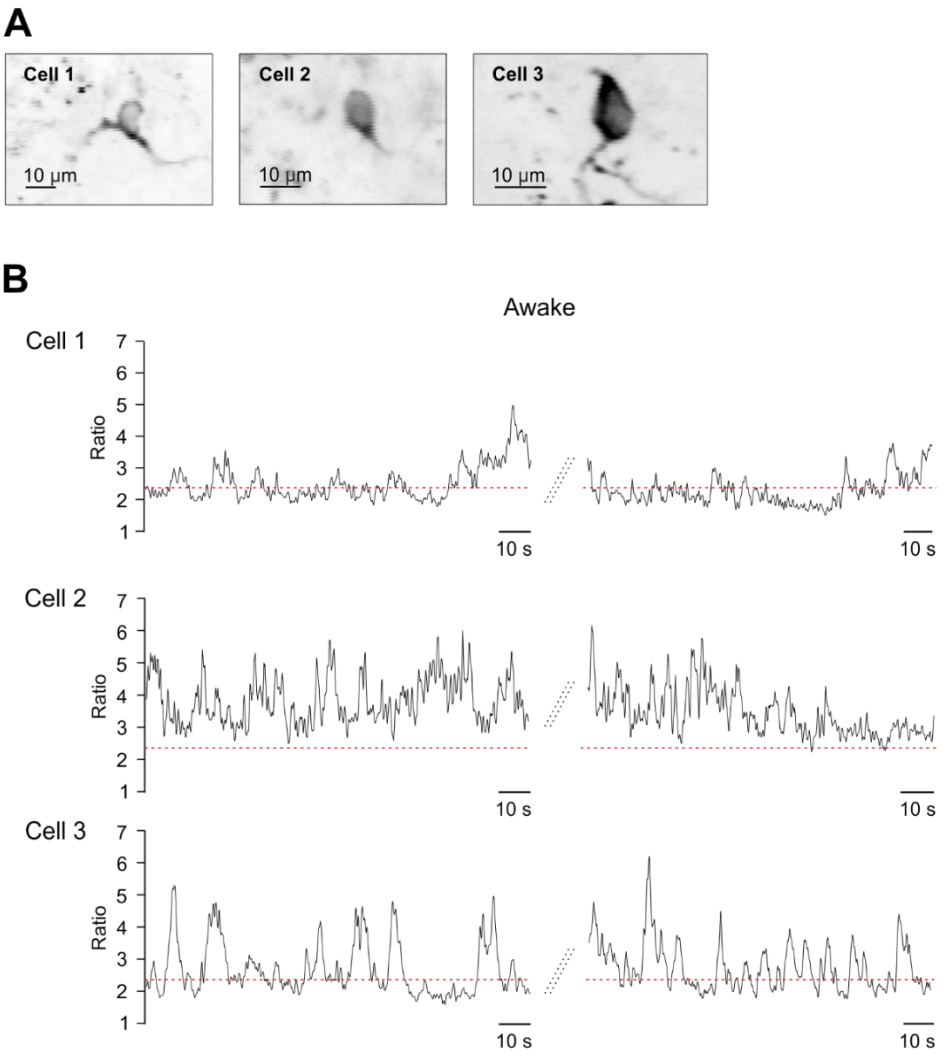

Figure 25. Spontaneous Ca^{2+} transients recorded from adult-born JNGs at DPI 20-22. (**A**) In-vivo images of Twitch-$2B^{+}$ adult-born JGNs at DPI 20-22. **(B)** Traces of spontaneous Ca^{2+} transients of adult-born JGNs at DPI 20-22. Red lines denote level of the ratio=2.4.

Despite changes in migratory behaviour [Liang et al. 2016] and the expression profile of neurochemical markers, occurring in adult-born JGNs between DPI 9 and DPI 20-24 (Figure 24), we did not observe any significant difference in the percentage of spontaneously active adult-born JGNs between cells studied in awake state at DPI 8-11 and DPI 20-22 (Figure 26). It should be noted that for this comparison we considered all adult-born JGNs studied at DPI 8-11 in awake state, also those that were not analysed under isoflurane-induced anaesthesia. Due to this reason the number of adult-born JGNs analysed at DPI 8-11 in Figure 25 (n=55 cells, 5 mice), is higher than the one analysed in Figures 16 – 19, where the number of cells selected for analysis was limited to only those JGNs that were studied both in awake state and under the anaesthesia.

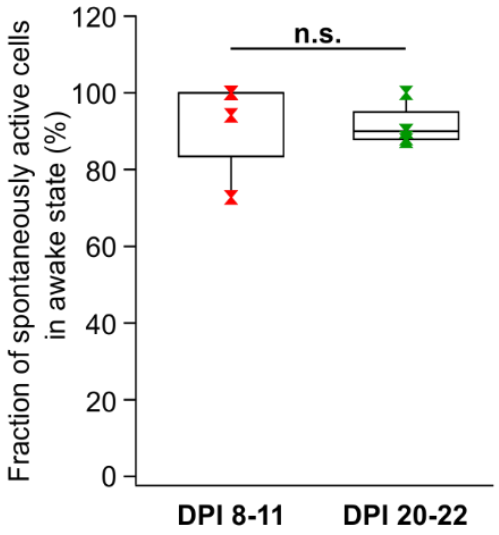

Figure 26. Percentage of spontaneously active adult-born JNGs at DPI 8-11 vs. DPI 20-22. Box plots illustrating the distributions of the percentage (per mouse) of spontaneously active adult-born JGNs at DPI 8-11 (n=55 cells, 5 mice) and DPI 20-22 (n=74 cells, 5 mice). Distributions are not significantly different (p=0.35, Mann-Whitney test).

Most of the spontaneously active cells recorded at DPI 8-11 and DPI 20-22 showed elevation of the cpVenus^{CD}/mCerulean3 ratio above the level of 2.4 only during the part of the recording time. However, the ratio traces of some of the spontaneously active adult-born JGNs were above the level of 2.4 during the whole time-lapse imaging session. To reveal fraction of cells showing such different patterns of intracellular calcium dynamics, adult-born JGNs studied in

awake state at DPI 8-11 and 20-22 were categorized into 3 groups on the basis of the behaviour of their cpVenus^{CD}/mCerulean3 ratio traces (Figure 27).

- Constantly active - the cpVenus^{CD}/mCerulean3 ratio trace was above the value of 2.4 during 99% of the imaging time
- Intermittently active - the cpVenus^{CD}/mCerulean3 ratio trace fluctuated going above and beyond the value of 2.4
- Silent - the cpVenus^{CD}/mCerulean3 ratio trace was beyond the value of 2.4 during the whole imaging session.

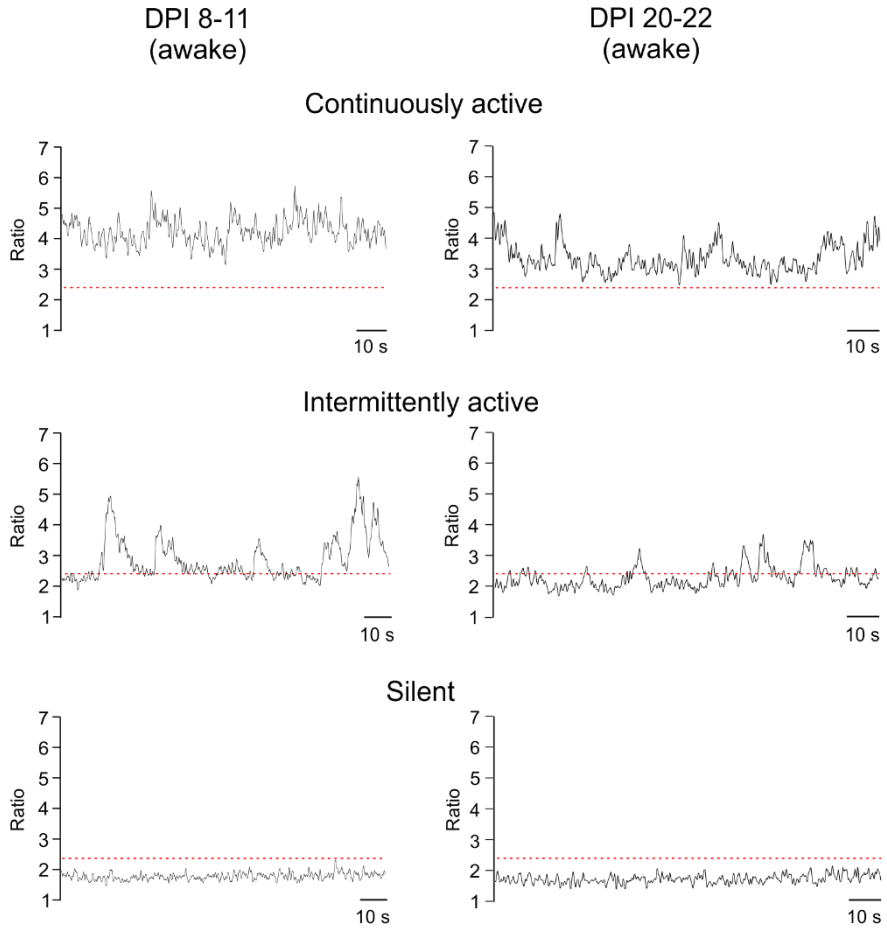

Figure 27. Patterns of the intracellular Ca^{2+} dynamics in adult-born JNGs at DPI 8-11 and DPI 20-22. Representative traces of spontaneous Ca^{2+} transients of adult-born JGNs at DPI 8-11 and DPI 20-22. Red lines denote level of the ratio=2.4.

Constantly active adult-born JGNs comprised 5.4% of all cells studied in awake state at DPI 8-11 (n=55 cells, 5 mice) and 14.9% of all adult-born JGNs studied in awake at DPI 20-22 (n=74 cells, 5 mice). Intermittently active cells comprised 87.3% and 75.7% of adult-born JGNs at DPI 8-11 and DPI 20-22 respectively, whereas 7.3% of adult-born JGNs at DPI 8-11 and 9.4% of adult-born JGNs at DPI 20-22 were silent. There was no significant difference between the distributions of constantly-, intermittently active and silent adult-born JGNs studied at DPI 8-11 and DPI 20-22 (Figure 28).

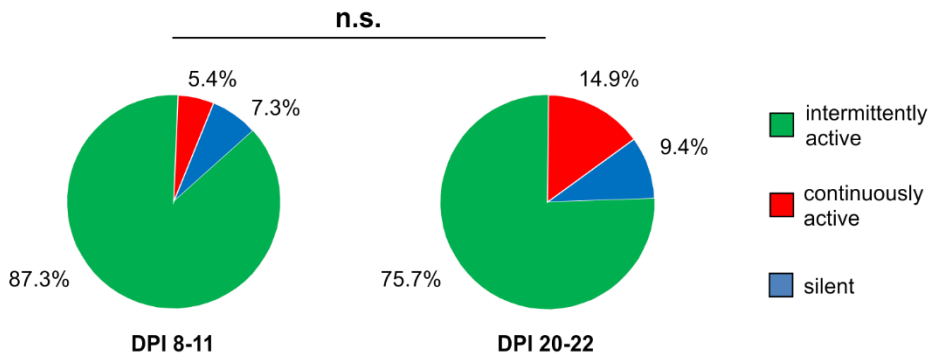

Figure 28. Patterns of intracellular Ca^{2+} dynamics in adult-born JNGs at DPI 8-11 vs. DPI 20-22 Pie charts showing the relative proportion of different activity patterns measured at the age of DPI 8-11 and DPI 20-22 in awake state. (DPI 8-11 n=55 cells, 5 mice; DPI 20-22 n=74 cells, 5 mice). The difference between the two distributions is not significant (p=0.194, Chi square test).

To test whether the properties of spontaneous calcium transients, such as the maximal ratio, the fraction of time spent in the active state, and the normalized area under the curve of the signal measured in awake state are different at DPI 20-22 vs. DPI 8-11, were analysed all adult-born JGNs that were active at DPI 8-11. Without silent cells but including those spontaneously active JGNs that were not measured under isoflurane. Therefore, the number of cells of this age in Figures 28-30 (n=51 cells, 5 mice) differs from the number of adult-born JGNs in the Figures 17-19 (n=44 cells, 5 mice).

The overall distributions of the values of maximal ratio acquired from all spontaneously active adult-born JGNs measured at DPI 8-11 (n=51 cells, 5 mice) and DPI 20-22 (n=67 cells, 5 mice) were similar. The number of cells from each mouse analysed in the DPI 8-11 group was 16, 10, 8, 8, 9. The number of cells from each mouse analysed in the DPI 20-22 group was 15, 9, 11, 14, 18. There was no significant difference in maximal ratio between the distributions of 5 medians calculated from the groups of cells for each of the 5 mice at DPI 8-11 and DPI 20-22 (Figure 29).

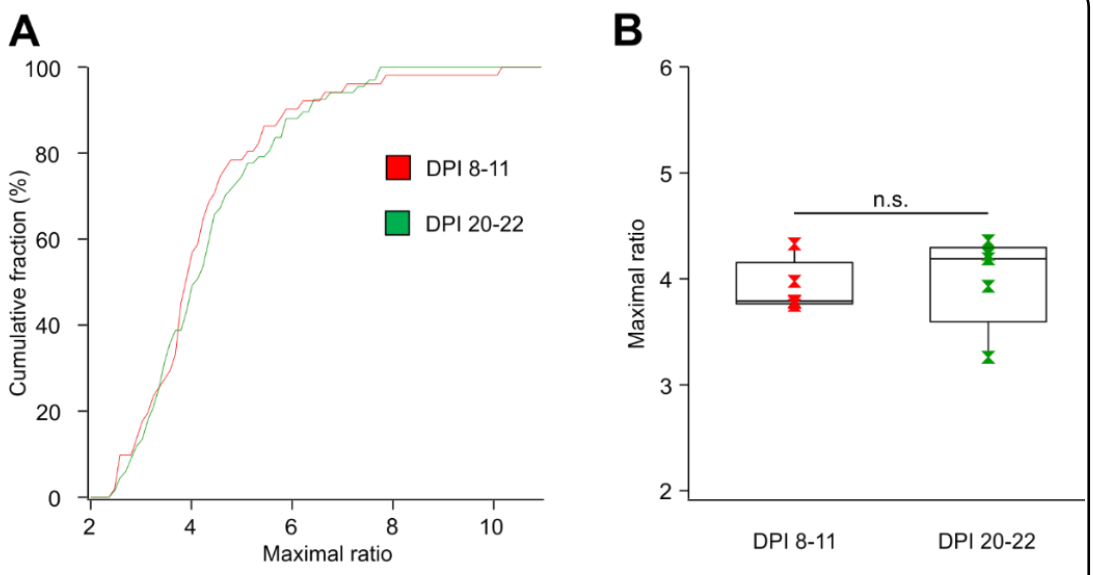

Figure 29. Maximal ratio of spontaneous Ca^{2+} transients of adult-born JGNs at DPI 8-11 vs. DPI 20-22 in awake state. (**A**) The cumulative probability histograms showing the overall distribution of the values of maximal ratio of spontaneous Ca^{2+} transients of adult-born JGNs measured at different age. (**B**) Box plots illustrating the distributions of medians calculated for the groups of cells from each mouse (DPI 8-11 n=51 cells, 5 mice; DPI 20-22 n=67 cells, 5mice). The two distributions are not significantly different (p=0.53, Mann-Whitney test).

However, the overall distributions of the fractions of time spent in active state, and the normalized area under the curve were dissimilar at DPI 8-11 and DPI 20-22 (Figures 30A, 31A). There was a significant difference between distributions of 5 medians of the values of these parameters calculated at DPI 8-11 vs. DPI 20-22 (Figures 30B, 31B).

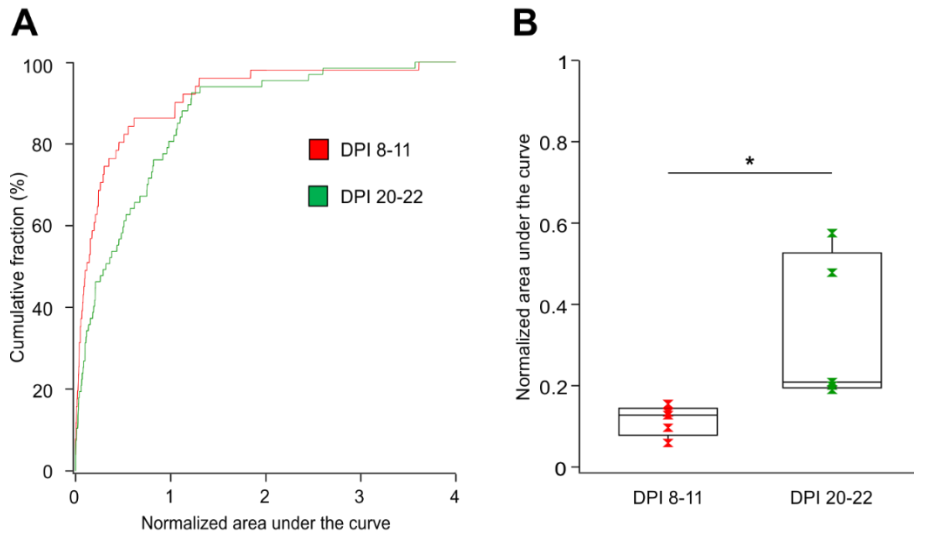

Figure 30. Normalized area under the curve measured from adult-born JGNs at DPI 8-11 vs. DPI 20-22. (**A**) The cumulative probability histograms showing the overall distribution of the normalized areas under the curve for adult-born JGNs measured at different age. (**B**) Box plots illustrating distributions of medians calculated for the groups of cells from each mouse (DPI 8-11 n=51 cells, 5 mice; DPI 20-22 n=67 cells, 5 mice). Asterisk denotes significant difference between the two distributions (p=0.012, Mann-Whitney test).

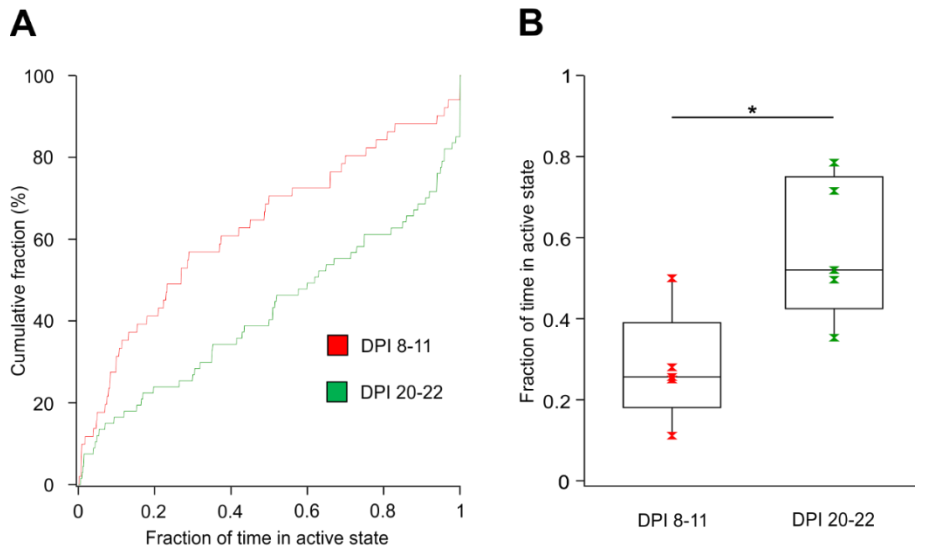

Figure 31. Fraction of time spent in the active state for adult-born JGNs at the age of DPI 8-11 vs. DPI 20-22. (**A**) The cumulative probability histograms showing the overall distribution of the values for fraction of time spent in active state for adult-born JGNs analysed at different age. (**B**) Box plots illustrating distributions of medians calculated for the groups of cells from each mouse (DPI 8-11 n=51 cells, 5 mice; DPI 20-22 n=67 cells, 5 mice). Asterisk denotes a significant difference between the two distributions (p=0.037, Mann-Whitney test).

Thus, spontaneous Ca^{2+} transients are present in adult-born JGNs at DPI 20-22. Percentage of spontaneously active adult-born JGNs, relative proportion of activity patterns and maximal ratio of the transients are similar between DPI 8-11 and DPI 20-22. However, spontaneous Ca^{2+} transients recorded at DPI 20-22 are significantly different from those recorded at DPI 8-11 in terms of the fraction of time spent in the active state, and the normalized area under the curve.

Discussion

In the present work in-vivo two-photon calcium imaging performed through implanted cranial widow showed that majority of immature adult-born JGNs exhibit spontaneous calcium transients in awake state. There was no significant difference in overall distributions of percentage of spontaneously active cells as well as in the median values of parameters chosen for characterisation of spontaneous calcium transients between awake state and isoflurane-induced anaesthesia.

In-vivo two-photon imaging performed under isoflurane-induced anaesthesia through acute craniotomy over the olfactory bulb showed that spontaneous calcium transients are blocked by addition of 2 µM tetrodotoxin to the standard extracellular solution.

Paired recordings of spontaneous activity in awake state and odorant-evoked calcium transients under 3 component anaesthesia revealed that substantial fraction of spontaneously active immature adult-born JGNs are able to respond to odorant presentation in front of the mouse's snout.

The overall dynamics of spontaneous calcium transients changed between 8-11 and 20-22 DPI. Similarly, we have also observed developmental changes in neurochemical marker expression between these two age groups.

In the developing nervous system spontaneous elevations of intracellular calcium concentration are believed to play an important role in neuronal differentiation. During embryonic development spontaneous calcium signals are involved in regulating migration, differentiation, and survival of immature neurons [Komuro and Rakic, 1996; Rosenberg and Spitzer, 2011; Uhlén P et al. 2015; Toth et al. 2016]. In analogy, it was shown that spontaneous calcium signals are present in adult-born neuroblasts migrating in the rostral extension of RMS in brain slices [Darcy et al. 2009]. However, it was not known whether spontaneous calcium signals are present in the immature adult-born JGNs during their integration into mature neuronal circuit under in-vivo conditions.

To the best of my knowledge, present work for the first time shows that immature adult-born JGNs (DPI 8-11) exhibit spontaneous calcium transients in-vivo, in awake state. This activity was abolished in the presence of TTX, thus suggesting that spontaneous calcium signals in adult-born JGNs are triggered by action potential firing. The latter, in turn, could be caused by network activity.

What can be the source of excitatory inputs to adult-born JGNs driving the spontaneous activity? As was mentioned above, circuit of JGNs comprise periglomerular neurons, short axon cells and external tufted cells. Periglomerular cells are the most numerous subpopulation of JGNs. Adult neurogenesis contributes most to periglomerular neurons [Lepousez et al. 2013]. External tufted cells considered to be a major excitatory element in the JGNs circuitry and these cells are able to generate bursts of action potential independently of synaptic inputs [Hayar et al. 2004]. Another potential source of excitatory network-driven stimulation of adult-born JGNs could be inputs form other regions of the brain, providing contextual information to the signal processing circuit of the olfactory bulb [Lazarini and Lledo, 2011].

In two-photon in-vivo imaging experiments performed under isoflurane-induced anaesthesia through acute craniotomy over the olfactory bulb only a few adult-born JGNs showed spontaneous calcium transients under control condition. This was in contrast to results acquired during awake measurements. Also, it was shown by [Wachowiak et al. 2013] that periglomerular neurons, exhibit different odorant-evoked responses in awake state vs. isoflurane-

induced anaesthesia. Nevertheless, results of paired two-photon in-vivo recordings performed from same immature adult-born JGNs neurons in awake state and under isoflurane-induced anaesthesia reveal no significant difference in overall distribution of the percentage of spontaneously active immature adult-born JGNs acquired from five mice in both conditions. Majority of adult-born JGNs, that were spontaneously active in awake, remain spontaneously active under isoflurane-induced anaesthesia in 4 out of 5 studied mice. However, in 1 mouse only 18.18% of those adult-born JGNs that were active in awake remained spontaneously active under anaesthesia. There was no significant difference between awake state and isoflurane-induced anaesthesia in distributions of median values pro mouse, of all three parameters chosen to characterise spontaneous calcium transients. Thus, the reduction in the number of spontaneously active immature adult-born JGNs observed in the acute experiments was probably due to acute trauma caused by the craniotomy.

In the developing nervous system both spontaneous and sensory-driven activities play an important role in the assembly of neuronal circuit and its refinement [Yhang and Poo 2001]. Spontaneous activity is evident already during embryonic development [Catsicas et al. 1998; Carey and Matsumoto, 1999; Spitzer 2006], whereas sensory-evoked activity is introduced later, during the postnatal period. Thus, in the developing nervous system spontaneous activity usually precedes the appearance of sensory-driven one. However, new neurons that are born during adulthood have to integrate into already mature environment with ongoing signal processing. In the present work in-vivo recordings of spontaneous activity and odorant-evoked calcium transients in the same immature adult-born JGNs revealed that considerable fraction of spontaneously active cells exhibit odorant-evoked calcium transients. So, there is a substantial overlap of both types of activity during integration period of adult-born JGNs. Moreover, we did not identify any properties of spontaneous calcium transients that could be predictive for odorant-responsiveness of a given immature adult-born JGN. There was no significant difference for all parameters chosen to characterise traces of spontaneous calcium signals

between odorant-responsive and odorant non-responsive immature adult-born JGNs.

Present work characterised maturational changes of the neurochemical profile of adult-born JGNs during their integration. At DPI 9, we revealed a very limited expression of mature neuronal markers calbindin, calretinin and tyrosine hydroxylase (TH), while almost all adult-born JGNs were positive for immature neuronal markers doublecortin and PSA-NCAM. These results are consistent with immature morphology of adult-born periglomerular cells at DPI 10 [Mizrahi 2007] and immature electrophysiological properties of adult-born periglomerular cells at DPI 7-14 [Grubb et al. 2008] as well as with active migratory behaviour that was shown for adult-born JGNs of this age [Kovalchuk et al. 2015; Liang et al. 2016]. At DPI 20-24, at the age when majority of adult-born JGNs stopped their migration in the glomerular layer [Liang et al. 2016], we revealed a substantial increase in percentage of adult-born JGNs positive for mature neuronal markers: calbindin, calretinin and tyrosine hydroxylase. Percentage of cells positive for calbindin, calretinin and TH among adult-born JGNs at DPI 20-24 revealed in the present work was similar to the percentage of neurons positive for calbindin, calretinin and TH among 30 days-old adult-born periglomerular cells, reported by Whitman and Greer [Whitman and Greer 2007a]. The fraction of TH-positive resident periglomerular neurons reported by Whitman and Greer was approximately two times lower than the fraction of TH-positive cells among 30 days old periglomerular neurons [Whitman and Greer, 2007a] and the fraction of TH-positive cells among DPI 20-24 adult-born JGNs revealed in the present work. The majority of resident periglomerular neurons was generated during embryonal development of the nervous system. Thus, our results support the suggestion the adult neurogenesis is more committed to generation of TH-positive GABAergic/dopaminergic periglomerular neurons than embryonic neurogenesis [Whitman and Greer, 2007a].

Despite the clear difference in neurochemical marker expression between adult-born JGNs at DPI 9 and DPI 20-24 revealed in the present work, and difference in the migratory behaviour of adult-born JGNs of corresponding age [Liang et al. 2016], there was no significant difference between percentage

of spontaneously active adult-born JGNs in awake state at DPI 8-11 vs. DPI 20-22. Also, there was no significant difference between proportions of silent, intermittently and continuously active cells at DPI 8-11 vs. DPI 20-22, as well as in the median values of maximal ratio of spontaneous calcium transients. However, there was a significant difference between spontaneous calcium signals at DPI 8-11 vs. DPI 20-22 in terms of fraction of time spent in the active state and the normalized area under the curve.

As was mentioned above, different patterns of spontaneous calcium transients can exert different effects on neuronal maturation during embryonic development [Rosenberg and Spitzer, 2011]. If this is also true for adult neurogenesis, it can be hypothesized that spontaneous calcium signals at DPI 8-11 and at DPI 20-22 are involved in different aspects of neuronal development. Spontaneous calcium transients in immature adult-born JGNs can be important for neuronal migration and acquisition of GABAergic phenotype, as such effects were shown in developing nervous system. In vitro study of intracellular calcium dynamics in migrating neurons cultured from developing mouse cerebellum [Komuro and Rakic 1996] revealed spontaneous calcium signals that were positively correlated with the rate of the movement of these cells. Furthermore, reduction of calcium influx by lowering extracellular calcium concentration resulted in altered rate of migration. Study of intracellular calcium dynamics in cultured embryonic Xenopus spinal neurons revealed that reduction of spontaneous calcium signals in these cells lead to a substantial decrease in number of GABAergic neurons. Whereas GABAergic phenotype could be rescued by artificial introduction of calcium spiking by the pulses of $CaCl_2$ [Gu and Spitzer 1995]. Consistently, it was shown that in embryonic Xenopus spinal cord neurons increase the intracellular concentration of GABA synthesizing enzyme glutamic acid decarboxylase (GAD) depending on the frequency of Ca^{2+} transients [Watt et al. 2000]. However, at DPI 20-22 adult-born JGNs already develop their neurotransmitter phenotype and majority of them stop migration inside of the glomerular layer. So, spontaneous calcium signals revealed in the majority of adult-born neurons of this age seem to have another role. This developmental stage is known to belong to a critical time

window for survival of adult-born JGNs [Whitman and Greer, 2007a]. Thus, spontaneous calcium signals potentially can be involved in life/death decisions of adult-born JGNs. This would be consistent with the hypothesis that successful integration of adult-born JGNs may be determined by the overall sum of activity in a given neuron during the critical period, regardless of its source – sensory-driven or spontaneous [Lin et al. 2010].

Summary

Adult mammalian brain is able to generate new neurons throughout life. Adult neural stem cells reside along the walls of the brain lateral ventricles – in a region called subventricular zone (SVZ) [Alvarez-Buylla and Garcia-Verduge 2002]. In the rodent brain thousands of neuroblasts that are born in the SVZ migrate into the olfactory bulb every day via a pathway that in called rostral migratory stream (RMS) [Alvarez-Buylla et al. 2001], to become functional interneurons – granule cells or juxtaglomerular neurons (JGNs) [Lledo et al. 2006]. In the developing nervous system spontaneous calcium transients are believed to be involved in the regulation of neuronal migration, differentiation and survival [Rosenberg and Spitzer, 2011]. In contrast to embryonic development, adult-born neurons have to integrate into the mature environment. It was shown that spontaneous calcium signals are present in adult-born neuroblasts migrating in the rostral extension of the olfactory bulb in-vitro [Darcy et al. 2009].

However, it was not known whether spontaneous calcium signals are present in the immature adult-born JGNs during their integration into mature neuronal circuit in vivo.

In the present work in-vivo two-photon calcium imaging was used to study spontaneous calcium signals in adult-born JGNs during their integration into the glomerular layer of the bulb. Adult-born JGNs were labelled via injection of lentivirus encoding the ratiometric fluorescent calcium sensor Twitch-2B into the rostral migratory stream. Twitch-2B is comprised of two fluorescent proteins: mCerulean3 and cpVenus^{CD} that are linked by a Ca^{2+}-binding region. Therefore, the dynamics of the intracellular calcium concentration is reflected in the corresponding dynamics of the cpVenus^{CD}/mCerulean3 ratio. In order to characterize properties of spontaneous calcium transients, values of the maximal cpVenus^{CD}/mCerulean3 ratio, fraction of time spent in active state and normalized area under the curve were calculated from corresponding traces of spontaneous calcium signals.

The results showed that majority of adult-born JGNs studied in awake state between 8th and 11th days post injection (DPI) exhibit spontaneous calcium transients.

Acute in-vivo experiments performed under isoflurane revealed that spontaneous calcium signals are blocked by an addition of 2 µM tetrodotoxin (TTX) into the standard extracellular solution.

Substantial fraction of immature adult-born JGNs (DPI 9-11) that were spontaneously active in awake sate, showed odorant-evoked calcium transients under 3 component anaesthesia. However, there was no significant difference in the properties of spontaneous calcium transients between odorant-responsive and odorant non-responsive cells.

At DPI 9, the majority of adult-born JGNs expressed immature neuronal markers, while expression of the mature markers was very limited. At DPI 20-24, the expression of mature neuronal markers was clearly upregulated. Despite the maturation of the neurochemical properties of adult-born JGNs, there was no significant difference in the percentage of spontaneously active adult-born JGNs in awake state at DPI 8-11 vs. DPI 20-22. However, some maturational dynamics was seen in the pattern of spontaneous calcium signals.

Thus, the present work provided in-vivo evidence of the presence of TTX-sensitive spontaneous calcium signals in immature adult-born JGNs; revealed substantial temporal overlap between spontaneous and sensory-evoked activity of immature adult-born JGNs and showed maturational dynamics of spontaneous calcium transients as well as neurochemical properties of adult-born JGNs during their integration into the mature environment of the adult brain.

Bibliography

1. Alvarez-Buylla A, Garcia-Verdugo JM & Tramontin AD (2001) A unified hypothesis on the lineage of neural stem cells. Nature Rev. Neurosci. 2, 287–293.
2. Alvarez-Buylla A and Garcia-Verdugo JM (2002) Neurogenesis in adult subventricular zone. The Journal of Neuroscience 22(3):629–634.
3. Alonso M, Viollet C, Gabellec MM, Meas-Yedid V, Olivo-Marin JC, Lledo PM (2006) Olfactory discrimination learning increases the survival of adult-born neurons in the olfactory bulb. J. Neurosci. 26, 10508–10513.
4. Alonso M, Lepousez G, Sebastien W, Bardy C, Gabellec MM, Torquet N, Lledo PM (2012) Activation of adult-born neurons facilitates learning and memory. Nat. Neurosci. 15, 897–904.
5. Altman J (1969) Autoradiographic and histological studies of postnatal neurogenesis IV. Cell proliferation and migration in the anterior forebrain, with special reference to persisting neurogenesis in the olfactory bulb. J. Comp. Neurol. 137, 433–458.
6. Altman J & Das GD (1965) Autoradiographic and histological evidence of postnatal hippocampal neurogenesis in rats. J. Comp. Neurol. 124, 319–335.
7. Baker H, Morel K, Stone DM, Maruniak JA (1993) Adult naris closure profoundly reduces tyrosine hydroxylase expression in mouse olfactory bulb. Brain Res 614:109-116.
8. Benninger RKP and Piston DW (2013) Two-Photon Excitation Microscopy for the Study of Living Cells and Tissues Curr Protoc Cell Biol.
9. Bonfanti L and Theodosiss DT (1994) Expression of polysialylated neural cell adhesion molecule by proliferating cells in the subependymal layer of the adult rat, in its rostral extension and in the olfactory bulb. Neuroscience Vol. 62. No. I, pp. 291-305.
10. Brill MS, Ninkovic J, Winpenny E, Hodge RD, Ozen I, Yang R, Lepier A, Gascón S, Erdelyi F, Szabo G, Parras C, Guillemot F, Frotscher M, Berninger B, Hevner RF, Raineteau O, Götz, M. (2009) Adult generation of glutamatergic olfactory bulb interneurons. Nat. Neurosci. 12, 1524–1533.
11. Brown JP, Couillard-Després S, Cooper-Kuhn CM, Winkler J, Aigner L, Kuhn H.G. (2003) Transient expression of doublecortin during adult neurogenesis. Journal of comparative neurology 467:1–10.
12. Carey MB, Matsumoto SG (1999) Spontaneous calcium transients are required for neuronal differentiation of murine neural crest. Dev Biol. 215(2):298-313.
13. Carleton A, Petreanu LT, Lansford R, Alvarez-Buylla A. & Lledo PM (2003) Becoming a new neuron in the adult olfactory bulb. Nat. Neurosci. 6, 507–518.

14. Catsicas M, Bonness V, Becker D, Mobbs P (1998) Spontaneous Ca2+ transients and their transmission in the developing chick retina. Curr Biol. 8(5):283-6.
15. Darcy DP and Isaacson JS (2009) L-type calcium channels govern calcium signaling in migrating newborn neurons in the postnatal olfactory bulb. J Neurosci. 29(8): 2510–2518.
16. Denk W, Strickler JH & Webb WW (1990) Two-photon laser scanning fluorescence microscopy. Science 248, 73–76.
17. Eriksson PS, Perfilieva E, Björk-Eriksson T, Alborn AM, Nordborg C, Peterson DA, Gage FH (1998) Neurogenesis in the adult human hippocampus. Nat Med. 4(11):1313-7.
18. Förster VT (1948) Zwischenmolekulare Energlewanderung undFluoresz. Annalen Dear Physik 2, 55–75.
19. Ghashghaei HT, Lai C, Anton ES (2007) Neuronal migration in the adult brain: are we there yet? Nature Reviews Neuroscience 8, 141-151.
20. Grubb MS, Nissant A, Murray K, and Lledo PM (2008) Functional maturation of the first synapse in olfaction: development and adult neurogenesis. J. Neurosci. 28, 2919–2932.
21. Guillemot F, Parras C. (2005) Adult neurogenesis: a tale of two precursors. Nature Neuroscience vol.8 number 7 p.846-848.
22. Gu X, Spitzer N (1995) Distinct aspects of neuronal differentiation encoded by frequency of spontaneous Ca2þ transients. Nature 375: 784–787.
23. Gu X, Spitzer N (1997) Breaking the code: regulation of neuronal differentiation by spontaneous calcium transients. Dev Neurosci 19: 33–41.
24. Hayar A, Karnup S, Ennis M and Shipley MT (2004) External Tufted Cells: a major excitatory element that coordinates glomerular activity. The Journal of Neuroscience, 24(30):6676 – 6685.
25. Kaplan MS (1984) Mitotitic neuroblasts in the 9-day-old and 11-month-old rodent hippocampus. J. Neurosci. 4, 1429–1441.
26. Kaplan MS & Hinds JW (1977) Neurogenesis in the adult rat: electron microscopic analysis of light radioautographs. Science 197, 1092–1094.
27. Kelsch W, Lin CW & Lois C (2008) Sequential development of synapses in dendritic domains during adult neurogenesis. Proc. Natl Acad. Sci. USA 105, 16803–16808.
28. Kelsch W, Lin CW, Mosley CP, Lois C (2009) A critical period for activity-dependent synaptic development during olfactory bulb adult neurogenesis. J Neurosci. 29(38):11852-8.
29. Kempermann G, Kuhn HG & Gage FH (1997) More hippocampal neurons in adult mice living in an enriched environment. Nature 386, 493–495.
30. Kiselycznyk CL, Zhang S, Linster C (2006) Role of centrifugal projections to the olfactory bulb in olfactory processing. Learn. Mem. 13, 575–579.
31. Kiyokage E, Pan YZ, Shao Z, Kobayashi K, Szabo G, Yanagawa Y, Obata K, Okano H, Toida K, Puche AC, Shipley MT (2010) Molecular identity of periglomerular and short axon cells. J. Neurosci. 30(3):1185-96

32. Komuro H, Rakic P (1996) Intracellular Ca2+ fluctuations modulate the rate of neuronal migration. Neuron 17(2):275-85.
33. Kopel H, Schechtman E, Groysman M & Mizrahi A (2012) Enhanced synaptic integration of adult-born neurons in the olfactory bulb of lactating mothers. J. Neurosci. 32, 7519–7527.
34. Kovalchuk Y, Homma R, Liang Y, Maslyukov A, Hermes M, Thestrup T, Griesbeck O, Ninkovic J, Cohen LB, Garaschuk O (2015) In vivo odourant response properties of migrating adult-born neurons in the mouse olfactory bulb. *Nat Commun*; 6:6349.
35. Kuhn HG, Dickinson-Anson H & Gage FH (1996) Neurogenesis in the dentate gyrus of the adult rat: age-related decrease of neuronal progenitor proliferation. J. Neurosci. 16, 2027–2033.
36. Lazarini F and Lledo PM (2011) Is adult neurogenesis essential for olfaction Is adult neurogenesis essential for olfaction? Trends Neurosci. 34(1):20-30.
37. Lepousez G, Valley MT, Lledo PM (2013) The impact of adult neurogenesis on olfactory bulb circuits and computations. Annu Rev Physiol. 75:339-63.
38. Liang Y, Li K, Riecken K, Maslyukov A, Gomez-Nicola D, Kovalchuk Y, Fehse B, Garaschuk O (2016) Long-term in vivo single-cell tracking reveals the switch of migration patterns in adult-born juxtaglomerular cells of the mouse olfactory bulb. Cell Research :1-17.
39. Lin CW, Sim S, Ainsworth A, Okada M, Kelsch W, Lois C. (2010) Genetically increased cell-intrinsic excitability enhances neuronal integration into adult brain circuits. *Neuron*. January 14; 65(1): 32.
40. Livneh Y, Adam Y, Mizrahi A (2014) Odor Processing by Adult-Born Neurons Neuron 81, 1097–1110.
41. Livneh Y, Feinstein N, Klein M, and Mizrahi A (2009). Sensory input enhances synaptogenesis of adult-born neurons. J. Neurosci. 29, 86–97.
42. Lledo PM, Alonso M, Grubb MS. (2006) Adult neurogenesis and functional plasticity in neuronal circuits. Nat. Rev. Neurosci. 7, 179–193.
43. Macrides F, Davis BJ, Youngs WM, Nadi NS, Margolis FL (1981) Cholinergic and catecholaminergic afferents to the olfactory bulb in the hamster: a neuroanatomical, biochemical, and histochemical investigation. J. Comp. Neurol. 203, 495–514.
44. Mandairon N, Jourdan F, Didier A (2003) Deprivation of sensory inputs to the olfactory bulb up-regulates cell death and proliferation in the subventricular zone of adult mice. Neuroscience 119, 507–516.
45. Mandairon N, Sacquet J, Jourdan F, Didier A (2006) Long-term fate and distribution of newborn cells in the adult mouse olfactory bulb: influences of olfactory deprivation. Neuroscience 141, 443–451.
46. Mandairon N, Sacquet J, Garcia S, Ravel N, Jourdan F, Didier A (2006) Neurogenic correlates of an olfactory discrimination task in the adult olfactory bulb. Eur J Neurosci 24:3578 –3588.
47. Mizrahi, A. (2007). Dendritic development and plasticity of adult-born neurons in the mouse olfactory bulb. Nat. Neurosci, 10, 444-452.

48. Moreno MM, Linster C, Escanilla O, Sacquet J, Didier A, Mandairon N (2009) Olfactory perceptual. learning requires adult neurogenesis. *Proc. Natl. Acad. Sci. USA* 106(42):17980–85.
49. Mouret A, Gheusi G, Gabellec M-M, de Chaumont F, Olivo-Marin JC, Lledo PM (2008) Learning and survival of newly generated neurons: when time matters. J. Neurosci. 28(45):11511–16.
50. Mouret A, Murray K, Lledo PM (2009) Centrifugal drive onto local inhibitory interneurons of the olfactory bulb. Ann. N. Y. Acad. Sci. 1170, 239–254.
51. Ninkovic J, Mori T & Götz M (2007) Distinct modes of neuron addition in adult mouse neurogenesis. J. Neurosci. 27, 10906–10911.
52. Panzanelli P, Fritschy JM, Yanagawa Y, Obata K, Sassoè-Pognetto M. (2007) GABAergic phenotype of periglomerular cells in the rodent olfactory bulb. J Comp Neurol. 502(6):990-1002.
53. Panzanelli P, Bardy C, Nissant A, Pallotto M, Sassoè-Pognetto M, Lledo PM, Fritschy JM (2009) Early synapse formation in developing interneurons of the adult olfactory bulb. J. Neurosci. 29, 15039–15052.
54. Parrish-Aungst S, Shipley MT, Erdelyi F, SzaboG. & Puche AC (2007) Quantitative analysis of neuronal diversity in the mouse olfactory bulb. J. Comp. Neurol. 501, 825–836.
55. Petreanu L and Alvarez-Buylla A (2002) Maturation and death of adult-born olfactory bulb granule neurons: role of olfaction. J. Neurosci. 22, 6106–6113
56. Petzold GC, Hagiwara A, Murthy VN. (2009) Serotonergic modulation of odor input to the mammalian olfactory bulb. Nat. Neurosci. 12, 784–791.
57. Ravel N, Akaoka H, Gervais R, Chouvet G. (1990) The effect of acetylcholine on rat olfactory bulb unit activity. Brain Res Bull. 24(2):151-5.
58. Rochefort C, Gheusi G, Vincent JD, Lledo PM (2002) Enriched odor exposure increases the number of newborn neurons in the adult olfactory bulb and improves odor memory. J. Neurosci. 22, 2679–2689.
59. Rosenberg S. and Spitzer N. (2011) Calcium Signaling in Neuronal Development. Cold Spring Harb Perspect Biol 3:a004259.
60. Saghatelyan A, Roux P, Migliore M, Rochefort C, Desmaisons D, Charneau P, Shepherd GM, Lledo PM (2005) Activity-dependent adjustments of the inhibitory network in the olfactory bulb following early postnatal deprivation. Neuron 46, 103–116.
61. Sakamoto M, Imayoshi I, Ohtsuka T, Yamaguchi M, Mori K, Kageyama R (2011) Continuous neurogenesis in the adult forebrain is required for innate olfactory responses. Proc. Natl Acad. Sci. USA 108, 8479–8484.
62. Seki T. (2002) Hippocampal adult neurogenesis occurs in a microenvironment provided by PSANCAM-expressing immature neurons. Journal of Neuroscience Research 69:772–783.
63. Shepherd GM, Chen WR and Greer CA (2004) The Synaptic Organization of the Brain pp. 165–217, Oxford University Press.
64. Shingo T, Gregg C, Enwere E, Fujikawa H, Hassam R, Geary C, Cross JC, Weiss S (2003) Pregnancy-stimulated neurogenesis in the adult female forebrain mediated by prolactin. Science 299, 117–120.

65. Spitzer NC (2006). Electrical activity in early neuronal development. Nature. 444(7120):707-12.
66. Svoboda K, Yasuda R (2006) Principles of Two-Photon Excitation Primer Microscopy and Its Applications to Neuroscience. Neuron 50, 823–839.
67. Thestrup T, Litzlbauer J, Bartholomäus I, Mues M, Russo L, Dana H, Kovalchuk Y, Liang Y, Kalamakis G, Laukat Y, Becker S, Witte G, Geiger A, Allen T, Rome LC, Chen TW, Kim DS, Garaschuk O, Griesinger C, Griesbeck O (2014) Optimized ratiometric calcium sensors for functional in vivo imaging of neurons and T lymphocytes. Nature methods 11: 175–182.
68. Toth AB, Shum AK, Prakriya M (2016) Regulation of neurogenesis by calcium signaling. Cell Calcium. 59(2-3):124-34.
69. Uhlén P, Fritz N, Smedler E, Malmersjö S, Kanatani S. (2015) Calcium signaling in neocortical development. Dev Neurobiol. 75(4):360-8.
70. Vucinić D, Cohen LB, Kosmidis EK (2006) Interglomerular center-surround inhibition shapes odorant-evoked input to the mouse olfactory bulb in vivo. J Neurophysiol. 95(3):1881-7.
71. Wachowiak M, Economo MN, Díaz-Quesada M, Brunert D, Wesson DW, White JA, Rothermel M (2013) Optical dissection of odor information processing in vivo using GCaMPs expressed in specified cell types of the olfactory bulb. J Neurosci. 33(12):5285-300.
72. Wachowiak M, Shipley MT (2006) Coding and synaptic processing of sensory information in the glomerular layer of the olfactory bulb. Seminars in Cell & Developmental Biology 17 411–423
73. Watt SD, Gu X, Smith RD, Spitzer NC (2000) Specific frequencies of spontaneous Ca2þ transients upregulate GAD 67 transcripts in embryonic spinal neurons. Mol Cell Neurosci 16: 376–387.
74. Whitman MC and Greer CA (2007a) Adult-Generated Neurons Exhibit Diverse Developmental Fates. Dev Neurobiol. 67(8):1079-93.
75. Whitman MC and Greer CA (2007b). Synaptic integration of adult-generated olfactory bulb granule cells: basal axodendritic centrifugal input precedes apical dendrodendritic local circuits. J. Neurosci. 27, 9951–9961.
76. Whitman MC, Greer CA (2009) Adult neurogenesis and the olfactory system. Progress in Neurobiology 89 162–175.
77. Winner B, Cooper-Kuhn CM, Aigner R, Winkler J, Kuhn HG (2002) Long-term survival and cell death of newly generated neurons in the adult rat olfactory bulb. Eur. J. Neurosci. 16, 1681–1689.
78. Yamaguchi M & Mori K (2005) Critical period for sensory experience-dependent survival of newly generated granule cells in the adult mouse olfactory bulb. Proc. Natl Acad. Sci. USA 102, 9697–9702.
79. Zhang LI, Poo MM (2001) Electrical activity and development of neural circuits. Nat Neurosci. 4 Suppl:1207-14.

Zusammenfassung

Das adulte Säugergehirn besitzt die Fähigkeit, zeitlebens neue Neuronen zu bilden. Adulte neuronale Stammzellen befinden sich entlang der Wände lateraler Gehirnventrikel, in der sogenannten subventrikulären Zone (SVZ) [Alvarez-Buylla und Garcia-Verduge 2002]. Im Nagergehirn wandern täglich Tausende dieser neu generierten Neuroblasten aus der SVZ in den Riechkolben, über einen Weg, der als rostraler migratorischer Strom (RMS) bezeichnet wird [Alvarez-Buylla et al. 2001]. Im Riechkolben differenzieren sich diese Zellen zu funktionellen Interneuronen, also zu Körnerzellen bzw. juxtaglomerulären Neuronen (JGN), aus [Lledo et al. 2006]. Während der embryonalen bzw. postnatalen Entwicklung spielen die spontan auftretenden zellulären Calcium-Transienten für die Regulation neuronaler Migration sowie für die Differenzierung und das Überleben von Neuronen eine wichtige Rolle [Rosenberg und Spitzer, 2011]. Im Gegensatz zur Embryonalentwicklung, müssen sich die im adulten Gehirn generierten Neuronen in ein reifes Netzwerk integrieren.

Es ist bisher jedoch nicht bekannt, ob unreife, im adulten Gehirn generierte JGN während ihrer Integration in das reife neuronale Netzwerk in vivo spontane Calcium-Signale aufweisen.

In der vorliegenden Arbeit wurden mittels in vivo Zwei-Photonenmikroskopie spontane Calcium-Signale der im adulten Gehirn generierten JGN während ihrer Integration in die glomeruläre Schicht des Riechkolbens untersucht. Für die Markierung dieser Zellen wurde eine stereotaktische Injektion eines Lentivirus in den RMS durchgeführt, welcher den ratiometrischen Calcium-Sensor Twitch-2B kodiert. Twitch-2B setzt sich aus zwei Fluoreszenzproteinen, mCerulean3 und cpVenus^{CD}, zusammen, welche über eine Calcium bindende Region miteinander verbunden sind. Daher reflektiert die Dynamik des cpVenus^{CD}/mCerulean3 Verhältnisses die Dynamik der intrazellulären Calcium-Konzentration. Um die Eigenschaften spontaner Calcium-Transienten zu charakterisieren, wurden der maximale cpVenus^{CD}/mCerulean3 Wert, der Anteil der Zeit im aktiven Zustand, und die

normalisierte Fläche unter der Kurve der jeweiligen spontanen Calcium-Signale bestimmt.

Die Ergebnisse zeigen, dass die Mehrheit der im adulten Gehirn generierten Neuronen im Wachzustand zwischen dem 8. und 11. Tag nach Injektion (DPI) spontane Calcium-Signale aufweist. Akute in vivo Experimente unter Isofluran-Anästhesie zeigten, dass die spontanen Calcium-Signale in Anwesenheit von 2 µM Tetrodotoxin (TTX) blockiert werden. Ein bemerkenswerter Anteil der im adulten Gehirn geborenen JGN (DPI 9-11), welche eine spontane Aktivität im Wachzustand aufwiesen, zeigten ebenfalls durch Duftstoffe hervorgerufene Calcium-Transienten unter 3-Komponenten-Narkose. Die Eigenschaften der spontanen Calcium-Transienten wiesen allerdings keine signifikanten Unterschiede zwischen Zellen, die auf Duftstoffe antworteten und denen, die nicht antworteten, auf.

9 Tage nach Injektion exprimierte die Mehrheit der im adulten Gehirn generierten Zellen Marker unreifer Neurone, während die Expression der Marker reifer Zellen niedrig war. 20 bis 24 Tage nach Injektion dagegen war die Expression der Marker reifer Neurone wesentlich höher. Trotz dieser Reifung neurochemischer Eigenschaften der im adulten Gehirn generierten JGN war der Anteil spontan aktiver Zellen 8 bis 11 Tage nach Injektion und 20 bis 22 Tage nach Injektion gleich. Es konnte jedoch eine gewisse Reifung in der Dynamik der Aktivitätsmuster spontaner Calcium-Transienten beobachtet werden.

Die vorliegende Arbeit dokumentiert das Auftreten TTX-sensitiver spontaner Calcium-Signale in unreifen, im adulten Gehirn generierten JGN in vivo und zeigt, dass im Gegenteil zu dem, was aus der embryonalen bzw. postnatalen Entwicklung bekannt ist, die spontane und sensorisch hervorgerufene Aktivität dieser Zellen gleichzeitig beobachtet werden kann. Zudem dokumentiert sie die Reifung der Dynamik spontaner Calcium-Transienten und neurochemischer Eigenschaften der im Adulten gebildeten JGN während ihrer Integration in die Umgebung des adulten Gehirns.

Publications

Part of the results presented in this thesis was published in the paper

Kovalchuk Y, Homma R, Liang Y, Maslyukov A, Hermes M, Thestrup T, Griesbeck O, Ninkovic J, Cohen LB, Garaschuk O (2015) In vivo odourant response properties of migrating adult-born neurons in the mouse olfactory bulb. *Nat Commun*; 6:6349.

Declaration of contribution

The dissertation work was carried out at the Institute of Physiology, Department of Neurophysiology, of the Eberhard Karls Universität Tübingen under the supervision of Professor Dr. Olga Garaschuk. The study was designed by Professor Dr. Olga Garaschuk.

After training by laboratory members Professor Dr. Olga Garaschuk, Dr. Yury Kovalchuk, Dr. Yajie Liang and PhD student Natalie Fomin-Thunemann I myself carried out viral injections into the rostral migratory stream, implantation of the cranial window over the mouse olfactory bulb, two-photon imaging of fixed stained tissue. In-vivo two-photon microscopy was performed together with Dr. Yury Kovalchuk and, in part, with a PhD student Xin Su. Immunostaining was done by our technical assistant Elizabeta Zirdum. Statistical analyses were carried out by myself under the supervision of Professor Dr. Olga Garaschuk.

I confirm that I wrote the manuscript myself under the supervision of Professor Dr. Olga Garaschuk and that any additional sources of information have been duly cited.

Acknowledgments

I want to express my gratitude to Professor Dr. Olga Garaschuk, Dr. Yury Kovalchuk and to the members of my doctoral committee Professor Dr. Stefan Liebau, and Professor Dr. Bernd Antkowiak. I would like to thank the whole team of Institute of Physiology, Department of Neurophysiology and Dr. Inka Montero. Without invaluable support of these people it would be not possible for me to accomplish this work.